We are IntechOpen, the world's leading publisher of Open Access books Built by scientists, for scientists

4,800
Open access books available

122,000
International authors and editors

135M
Downloads

Our authors are among the

154
Countries delivered to

TOP 1%
most cited scientists

12.2%
Contributors from top 500 universities

CLARIVATE ANALYTICS BOOK CITATION INDEX INDEXED

WEB OF SCIENCE™

Selection of our books indexed in the Book Citation Index in Web of Science™ Core Collection (BKCI)

Interested in publishing with us?
Contact book.department@intechopen.com

Numbers displayed above are based on latest data collected.
For more information visit www.intechopen.com

10

Advanced Electron Microscopy Techniques on Semiconductor Nanowires: from Atomic Density of States Analysis to 3D Reconstruction Models

Sònia Conesa-Boj[1], Sònia Estradé[1], Josep M. Rebled[1], Joan D. Prades[1], A. Cirera[1], Joan R. Morante[1,2], Francesca Peiró[1], and Jordi Arbiol[1,3,*]

[1]*Dept. d'Electrònica, Universitat de Barcelona*

[2]*IREC, Catalonia Institute for Energy Research*

[3]*ICREA Research Professor at Institut de Ciència de Materials de Barcelona, CSIC*

Spain

1. Introduction

Technology at the nanoscale has become one of the main scientific world challenges as new quantum physical effects appear and can be modulated at will (Kastner, 1992). Superconductors, materials for spintronics, electronics, optoelectronics, chemical sensing, and new generations of functionalized materials are taking advantage of the low dimensionality, improving their properties and opening a new range of applications (De Franceschi et al., 2003; Samuelson et al., 2004; Fischer et al., 2006; Pettersson et al., 2006; Wang et al., 2006; Hernández-Ramírez et al., 2007; Qin et al., 2007; Appenzeller et al., 2008; Boukai et al., 2008; Hochbaum et al., 2008; Wang et al., 2008; Colombo et al., 2009; Thunick et al., 2009). These new materials for future applications are being synthesized at the nanoscale (ultrathin layers, nanoparticles, nanowires or nanotubes functionalized). Among all these new materials, one-dimensional (1D) nanostructures such as nanowires, are one of the most used and promising morphologies (Lieber, 2003; Yang, 2005; Thelander et al., 2006; Lieber & Wang, 2007). Groups all around the world in the area of materials science, physics, chemistry and biology work in close collaboration with nanoscopy tools as there is a critical need for the structural, chemical and morphological characterization of the synthesized nanostructures at atomic scale in order to correlate these results with the physical and chemical properties and functionalities they present. In order to obtain an accurate control and understanding of these new materials properties, it is essential to access their structure and chemistry at atomic scale. Electron Microscopy and more precisely (scanning) transmission electron microscopy ((S)TEM) and electron spectroscopy related techniques (also known as electron nanoscopies) have thus a preeminent role in advanced materials science. Recent developments in electron microscopy, such as aberration correctors and monochromators are allowing us to reach sub-angstrom and sub-eV, spatial and energy resolutions, respectively. In addition to these advances, the possibility to obtain 3D models of our nanostructures by means of electron tomography, have shown that Electron Microscopy related techniques are the most promising to fully characterize complex

Source: Nanowires, Book edited by: Paola Prete,
ISBN 978-953-7619-79-4, pp. 414, March 2010, INTECH, Croatia, downloaded from SCIYO.COM

nanostructures. In the present chapter we will show how advanced electron microscopy techniques can be applied to obtain a deeper characterization of complex structures in semiconductor nanowires. The chapter will be distributed in two parts: in the first one, we will show the advantages of using aberration-corrected STEM and monochromated electron energy loss spectroscopy (EELS) in order to deeply characterize 1-D nanostructures at atomic scale. As an advanced example of how these techniques can improve Nanowire characterization, we will show how they can allow the local analysis of the atomic scale modifications in the local density of states that occur in a complex system in which high Mg-doping induces formation of transversal twin defects (perpendicular to the growth axis) on GaN Nanowires (NWs). Formation of these defects generates local structural phase changes, thus implying a different optoelectronic behavior of the nanowires, induced by the local change in the material bandgap. The considered techniques can allow measuring the bandgap exactly in every atomic column, thus leading to a complete characterization. In the second part of the chapter, we will focus on how 3D reconstruction of 1D nanostructures by means of electron tomography can improve the morphological characterization at the nanoscale. As advanced examples of this part, we will show how to obtain 3D models of complex coaxial nanowire heterostructures.

2. Aberration-corrected scanning transmission electron microscopy and monochromated electron energy loss spectroscopy

2.1 State of the art

Nowadays, given the eventual reduction in scale of the challenges at hand and the progressive instrumental advances that have taken place in microscopy in general and in EELS in particular, EELS has become one of the most crucial tool in materials science and even the life sciences (Calvert et al., 2005; Pan et al., 2009). As EELS is performed in the Transmission Electron Microscope (TEM), it benefits from the very high spatial resolution that can be achieved with electron optics, which can focus the electron beam to form a subnanometric probe. In particular, if a field emission gun is used, sufficient current can be obtained for a 1 nm probe. Within aberration-corrected instruments, this figure can be reduced to 0.1 nm. In addition, EELS can be easily combined with structural information as obtained from the TEM imaging and diffraction modes, and even with complementary X-ray energy-dispersive spectroscopy (EDXS) if needed. There is a fundamental limit to the minimum lateral resolution that can be achieved by EELS, irrespective of the electron optics. This limit is given by the delocalisation produced in inelastic scattering, and depends on the energy loss (the lower the loss, the greater the delocalisation) (Egerton, 1996). Yet, fortunately, this limit does not prevent from getting EELS signal from single atom columns at core-loss (Allen, 2003) or subnanometric resolution in low-loss experiments (Grogger, 2005). With the recent advances in instrumentation (spherical aberration correctors, electron monochromators, new energy filters and CCD detectors) EELS experiments can now be performed with a spatial resolution well below 0.1 nm and an energy resolution better than 0.1 eV. One of the instrumental highlights in the history of TEM is the recent introduction of systems to compensate for spherical and even chromatic aberrations (Haider et al., 1998; Batson et al., 2002). Using aberration corrected microscopy, an electron probe smaller than 1 Å can be achieved, which allows imaging of single atoms, clusters of a few atoms, and atomic columns. A multipole corrector built into the illumination system of a STEM increases the image resolution and allows more current to be focused in a given probe. This

is of great importance for spectroscopy, as both lateral resolution and signal-to-noise ratio are enhanced. If EELS presents a lower energy resolution when compared to other spectroscopies as XAS, the limitation does not lie in the capabilities of the spectrometers, but in the energy width of the electron source. This energy dispersion is typically 1–2 eV for a thermionic source, 0.5–1 eV for a Schottky or hot field-emission tip and around 0.3-0.35 eV for a cold field-emission tip. For comparison, synchrotron X-ray sources and beam-line spectrometers commonly provide a resolution below 0.1 eV for absorption spectroscopy, and even below 1 meV in certain cases (Egerton, 2003). In order to reduce the source energy spread, monochromators have been recently introduced. Nowadays, the monocromators yield a beam current in the order of several 100 pA (Tsuno, 2000; Egerton, 2003; Sigle, 2005). In particular, and due to all these achievements, HREELS associated to STEM in HRHAADF mode, can be used to solve the local electronic properties in nanostructured materials. In this way, bulk plasmon peak position can be used as an indirect compositional measure, and has been extensively used as a local chemical characterization tool, especially in the case of semiconductors. It can be primarily used as an identification tag for determining which compound is there at a given region of the studied specimen (Topuria et al., 2003; Irrera et al., 2005). As the plasmon peak position depends on the lattice parameter (as well as the bandgap energy and the dielectric constant) it can also give an indirect measure of structural properties (Shen et al., 2000; Sanchez et al., 2006). The need for characterization techniques that provide precise information regarding the bandgap and general optical properties at high spatial resolution seems to be out of question, given the scaling down that has taken place in the field of materials science and the rapidly widening use of nanostructures. In this sense, standard optical techniques such as vacuum ultra-violet spectroscopy do not provide the spatial resolution required to probe a material on the nanometer scale. Low-loss EELS seems to be a most fitting technique for the local characterization of optoelectronic properties at the nanoscale. For insulators or semiconductors with a sufficiently wide bandgap (that can be less than 1 eV using a monochromated STEM (Erni & Browning, 2005)), interband transitions can be observed in the EELS spectrum. It is possible to identify through EELS the bandgap energy of given nanostructures (Kuykendall et al., 2007; Arenal et al., 2008; Iakoubovskii et al., 2008). It is also possible to assess the existence of localized states within the bandpgap, which may be due to the presence of dislocations or other kinds of defects, for instance (Batson et al., 1986; Xin et al., 2000), which create new energy levels in the local DOS.

2.2 Particular case: Local electronic properties of Mg doped GaN NWs

In recent years much attention has been focused on the growth of quasi-one-dimensional (1D) nanostructures for the controlled fabrication of nanodevices (Arbiol et al., 2002; Hernandez-Ramirez et al., 2007; Hochbaum et al., 2008; Nesbitt, 2007; Stern et al., 2007). In particular, III-nitrides (InN, GaN, AlN and their alloys) have shown promising properties. Their direct band gap can be controlled from 0.7 eV (InN) to 3.4 eV (GaN) and to the deep UV spectral range of 6.0 eV (AlN). This makes them excellent candidates for the fabrication of heterostructures for optoelectronic applications, such as light emitting diodes, laser diodes, or quantum well infrared photodetectors as well as high electron mobility transistors. The synthesis of p-type 1D nanostructures based on these III-nitrides is still a challenging topic. To exploit these material properties also in nanoscaled devices, catalyst-induced processes like the vapour liquid solid (VLS) mechanism (Wagner & Ellis, 1964;

Morral et al., 2007), using metal droplets like Au, Ni (Chen et al., 2001; Kim et al., 2003), or Fe (Chen et al., 2001) as catalysts have been developed for the growth of GaN nanorods (NRs) or nanowires (NWs) with vertical orientation with respect to the substrate, with horizontal orientation, or as free structures. GaN NWs grown by laser assisted catalytic growth have been reported and heterodiodes have been realized by deposition of n-type GaN NWs on p-type Si substrates (Huang et al., 2002). However, for the integration of more complex structures such as p–n junctions or quantum wells, and in order to avoid the negative effects of catalysts in group III–V NRs or NWs, molecular beam epitaxy (MBE) is the growth method of choice (Calleja et al., 2000; Colombo et al. 2008; Morral et al., 2008b). As mentioned above, for the realization of nanoelectronic devices doping is one of the most important issues. In the case of Mg doped (p-type) GaN NRs and NWs, only a few studies have been devoted to analyze their optoelectronic (Furtmayr et al., 2008a; Furtmayr et al., 2008b; Park et al., 2006a; Zhong et al., 2003; Lai et al., 2006; Pal et al., 2006), transport, and electronic properties (Cheng et al., 2003; Zhong et al., 2003; Park et al., 2006b). Some of these works have provided limited information on the morphology (Park et al., 2006a) and crystal structure (Cheng et al., 2003; Zhong et al., 2003; Cimpoiasu et al., 2006) of the Mg doped GaN NRs and NWs. In addition, the analysis of GaN NWs as a model system for single crystals with a very low defect density can also contribute to solving some of the still existing technological problems of p-type doping of GaN with Mg in general. To this end, in the following we will show how combination of atomically resolved high resolution electron energy loss (EEL) measurements with specific *ab-initio* calculations can be a useful way to demonstrate that the presence of Mg atoms during the growth of GaN nanowires results in direct structural and morphological modifications with significant effects on the local electronic structure.

2.3 Experimental details: Growth method

Gallium nitride nanowires were grown using plasma assisted molecular beam epitaxy (PAMBE). Nitrogen radicals were supplied by an Oxford Applied Research RF-plasma source whereas for Ga and Mg thermal effusion cells were used. Low resistivity n-type Si(111) substrates were etched in 5% hydrofluoric acid for 10 s to remove the surface oxide layer prior to transfer into the load lock chamber. For all samples a substrate temperature of 790 ^{o}C, a nitrogen pressure of 2.7×10−5 mbar and a Ga beam equivalent pressure (BEP) of 3.3 × 10^{-7} mbar was used. The substrates were exposed to the nitrogen plasma at a temperature of 790 ^{o}C for 2 min directly before GaN growth. For the magnesium doped samples the Mg effusion cell temperature (TMg) was varied between 205 ^{o}C and 355 ^{o}C, corresponding to a BEP of 1×10^{-11} mbar to 2×10^{-8} mbar, respectively. Growth duration was 90 min unless mentioned otherwise. Samples were grown by Florian Furtmayr, Christoph Stark, Martin Stutzmann and Martin Eickhoff (Walter-Schottky-Institut, Technische Universität München) and Andreas Laufer (I Physikalisches Institut, Justus-Liebig-Universität).

2.4 Transmission electron microscopy characterization

In order to analyze the influence of the Mg doping on the atomic structure of the Mg NWs, selected area electron diffraction (SAED) patterns were obtained on several samples, prepared in XTEM geometry (Fig. 1. SAED analysis). Fig. 1.(a) shows a bright field STEM (BFSTEM) general view of the undoped GaN NWs. Its corresponding SAED pattern is displayed in Fig. 1.(b).

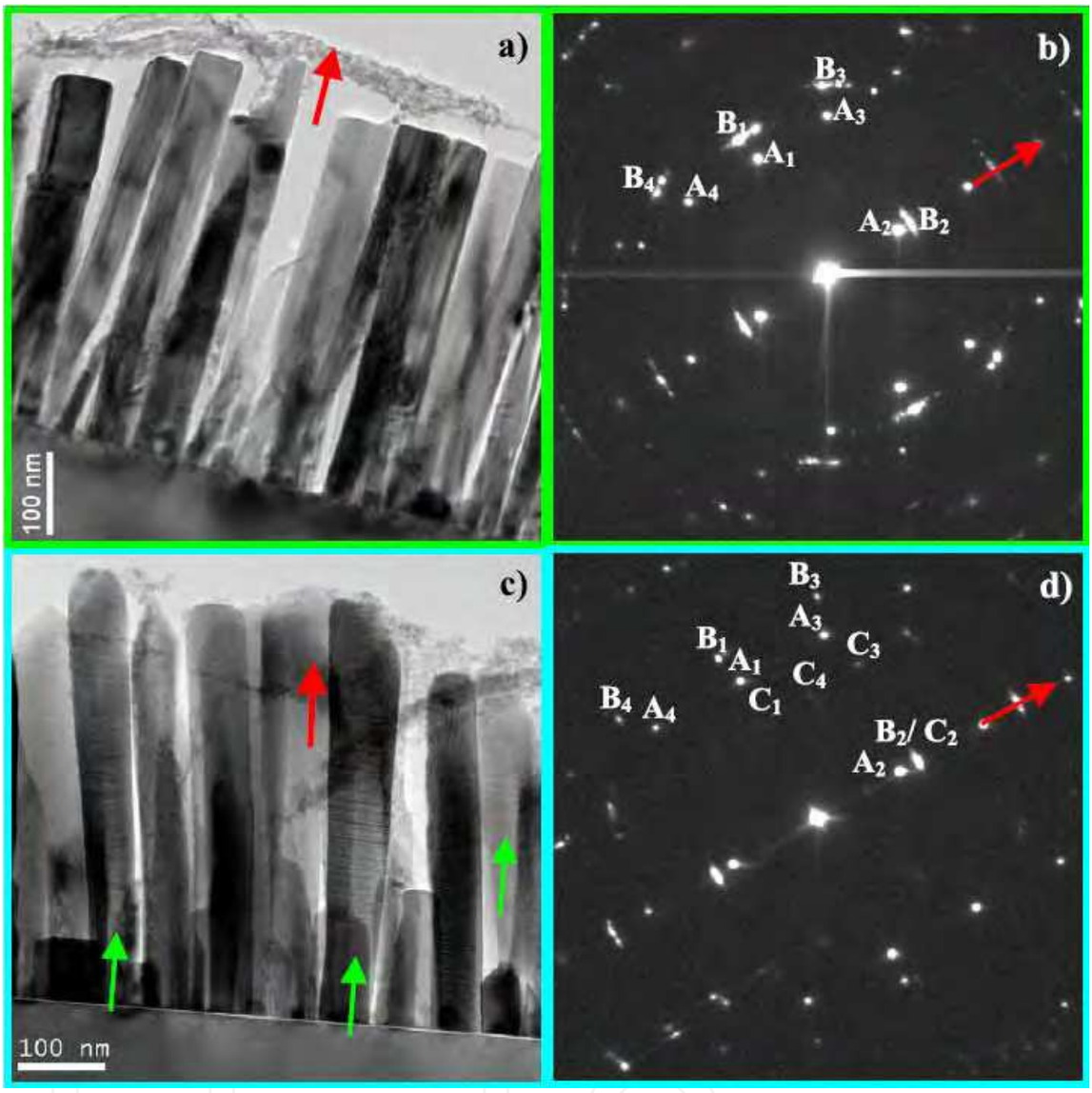

Fig. 1. SAED analysis

On the other hand, Fig. 1.(c) shows a BFSTEM general view of the highly Mg doped (TMg = 355 ºC) GaN NWs. Some of the NWs present twin defects (marked with green arrows). In this case, Fig. 1.(d) displays its SAED pattern. A new crystal orientation appears in this case, that has been related to the twinned NWs (spots labelled as C). Top arrows (red) are pointing to the same equivalent growth direction in SAED patterns and BFSTEM micrographs. After this analysis (see the corresponding indexation in Table 1. SAED patterns indexation) it was observed that GaN NWs follow a preferential epitaxial relationship versus the Si substrate, namely: (0001)[0-110] GaN // (111)[-1-12] Si (Arbiol et al., 2009). Undoped GaN NWs appear to be defect-free, whilst Mg doped samples present some NWs with twin (T) defects along the growth axis, as shown in Fig. 1.(a) and (b) -some twinned NWs have been marked with green arrows in Fig. 1.(c). When a SAED pattern of a NW region populated with few twinned NWs is obtained, a new orientation relationship

superimposed to the one found for undoped samples can be observed. As shown in Fig. 1.(d), the new spots (indexed in Table 1. SAED patterns indexation), labeled as C_n, are rather weak. The presence of these weak spots can be attributed to the presence of Ts in the NWs. The new epitaxial relationship which is found is: (0001)[1-210]GaN // (111)[-1-12]Si. The twinned NWs still grow along the [0001] direction; however, they are rotated 30º along the growth axis with respect to the non-twinned NWs.

Spot #	**d (nm)**	**(deg) versus spot A_1**	**Indexation**
A1	1.92	–	(2-20)
A2	3.13	90	(111)
A3	1.64	31	(3-11)
A4	1.64	31	(1-3-1)
Zone axis: [-1-12] Si			

Spot #	**d (nm)**	**(deg) versus spot B_1**	**Indexation**
B1	1.55	–	(-2110)
B2	2.59	90	(0002)
B3	1.30	32	(-2112)
B4	1.30	32	(-211-2)
Zone axis: [0-110] GaN			

Spot #	**d (nm)**	**(deg) versus spot C_1**	**Indexation**
C1	2.76	–	(-1010)
C2	2.59	90	(0002)
C3	1.89	43	(-1012)
C4	2.44	62	(-1011)
Zone axis: [1-210] GaN			

Table 1. SAED patterns indexation

The density of twins dramatically increases with increasing Mg concentration and, thus, the formation of twins can be directly correlated to the increasing presence of Mg. Twin defects along the growth axis have been commonly observed in some other one-dimensional semiconductor nanostructures such as in III–V NWs (Huang et al., 2002; Mikkelsen et al., 2004; Johansson et al., 2006; Davidson et al., 2007; Karlsson et al., 2007; Arbiol et al., 2009), or even in Si NWs (Arbiol et al., 2007; Arbiol et al., 2008b).

High resolution TEM (HRTEM) analysis (Fig. 2. HRTEM analysis of the highly Mg-doped GaN NWs) confirms that NWs with Ts grow in the (0002)[1-210]GaN // (111)[-1-12]Si orientation and are rotated 30º from the defect-free NWs. As shown in Fig. 2.(e), red arrows are pointing towards GaN(0001) wurtzite planes, while the cyan ones are pointing to the GaN twinned planes (in particular to a triple-twin region). As observed, the stacking of the planes is different in the twinned regions. On the other hand, an amorphous layer between the substrate and the GaN NW is apparent in Fig. 2.(a). Core-loss EELS quantification along the interface was carried out to find out the chemical nature of this amorphous layer. As Si

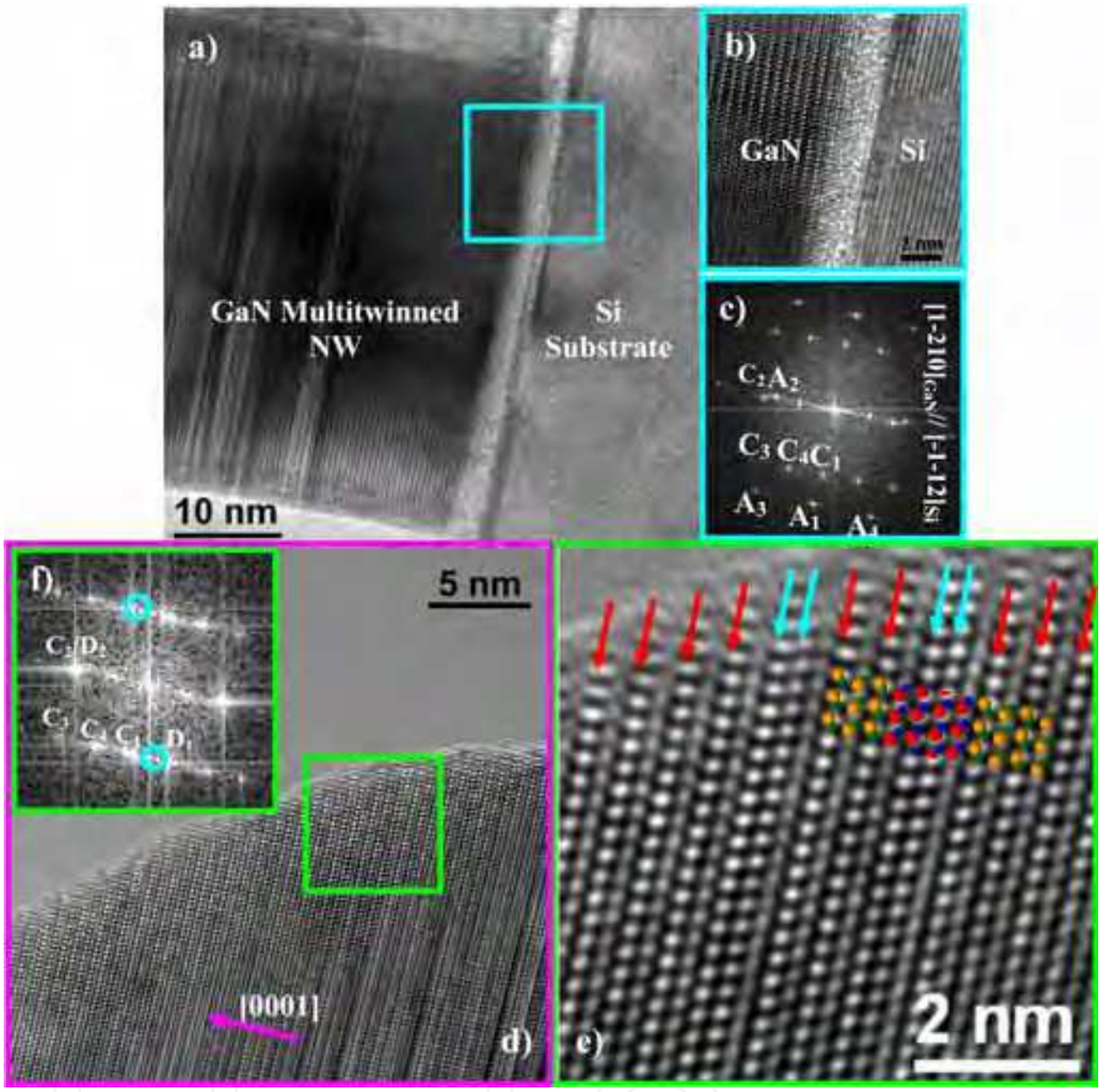

Fig. 2. HRTEM analysis of the highly Mg-doped GaN NWs

$L_{2,3}$ and Ga $M_{2,3}$ edges overlap, quantification was not carried out in the usual manner (computing background subtracted integrated signals for each element, sigma correcting them and dividing them by each other), but rather treating the overlapping region as a linear combination of the Si and Ga edges. This way, it was found that the amorphous layer contained 50 ± 5 % of Si, 50 ± 5 % of N and no Ga (Fig. 3. GaN/Si interface EELS analysis). This Si nitride layer was very likely created during the nitridation process that occurred during the first growth steps. A scheme of the twin formation is also shown (Fig. 4. Twin formation scheme). Fig. 4.(a) represents the conventional GaN wurtzite (WZ) structure, while in Fig. 4.(c) the formation of a single twin, equivalent to a 180º rotation in the WZ structure around the [0001] growth axis, is shown. It is important to point out that the consecutive stacking of [0001] axial twins leads to the formation of the GaN zinc-blende (ZB) structure, which is cubic instead of hexagonal (Fig. 4.(b) for a scheme of the GaN ZB structure).

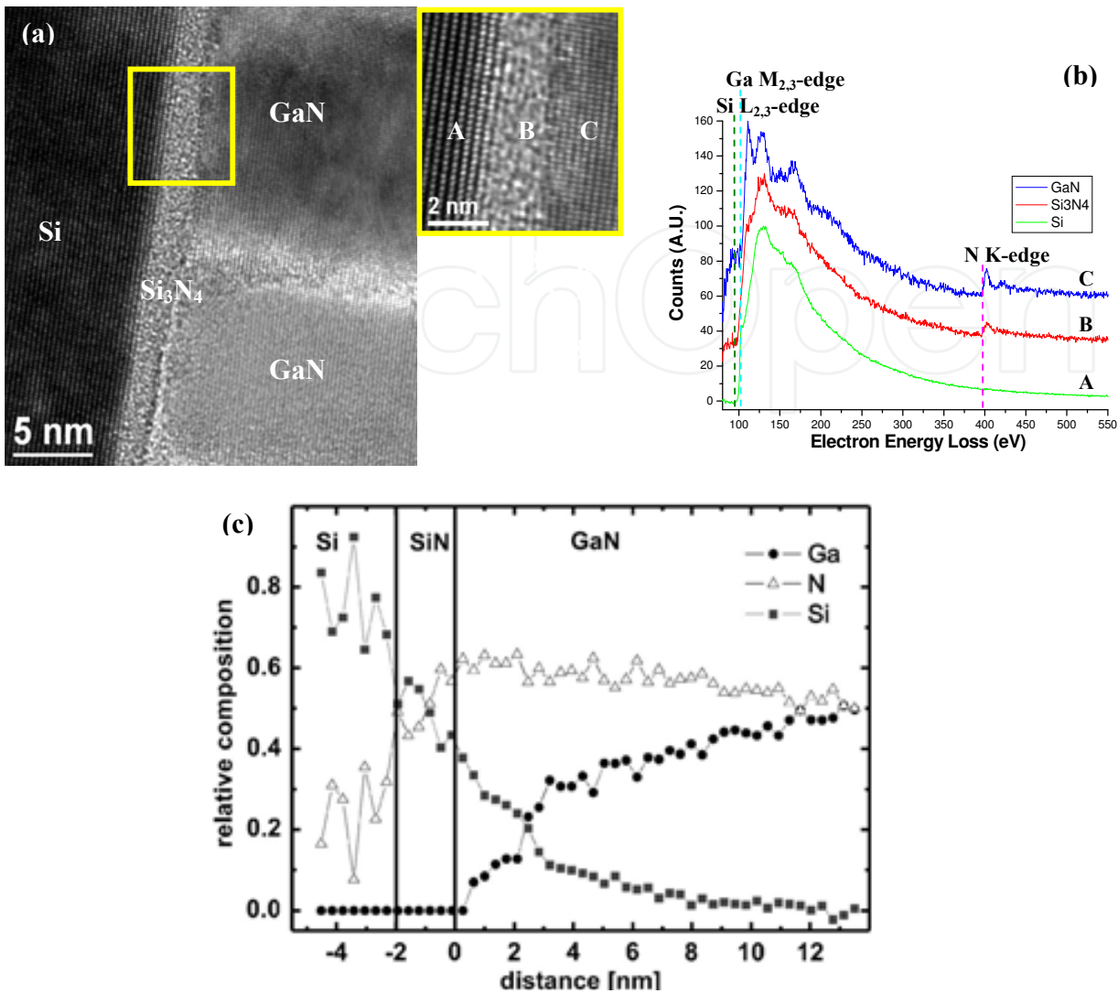

Fig. 3. GaN/Si interface EELS analysis. For Fig. 3.(c) see (Arbiol et al., 2008b).

In particular, it is displayed how a triple-twin creates a three-cell ZB domain (Figs. 2.(e) & 4.(e)). In this way, in the power spectrum shown in Fig. 2.(f), the D1 spot corresponds to the (-11-1) GaN ZB plane, while the D2 spot is the (111) plane. The appearance of alternating wurtzite and zinc-blende structures due to the presence of twins has been widely reported for III–V NWs (Banerjee et al., 2006; Ihn et al., 2006; Arbiol et al., 2008b) and the change of crystal phases in 1D nanostructures due to twinning is a widespread phenomenon in several materials (Arbiol et al., 2008a). In addition, the formation of wurtzite and zinc-blende heterostructures in a chemically homogeneous nanowire material is a hot scientific topic as it is opening up new possibilities for band-structure engineering (Algra et al., 2008; Arbiol et al., 2008b; Bao et al., 2008). These heterostructures can have dramatic implications on the electronic properties of the NWs, as a change in the crystal structure also implies a variation in the density of states and thus on the carrier transition energy.

In the present case, due to the different band gap, the resulting inclusion of ZB GaN in the WZ GaN NW creates quantum well regions along the NW axis. In a recent work (Bao et al., 2008), it was shown how the presence of twinned planes between WZ quantum domains in InP NWs (they attributed it to WZ–ZB alternance) could influence their photoluminescence properties.

In their case, the excitation power dependent blueshift of the observed photoluminescence could be explained in terms of the predicted staggered band alignment of the rotationally twinned ZB/WZ InP heterostructure and of the concomitant diagonal transitions between localized electron and hole states responsible for radiative recombination.

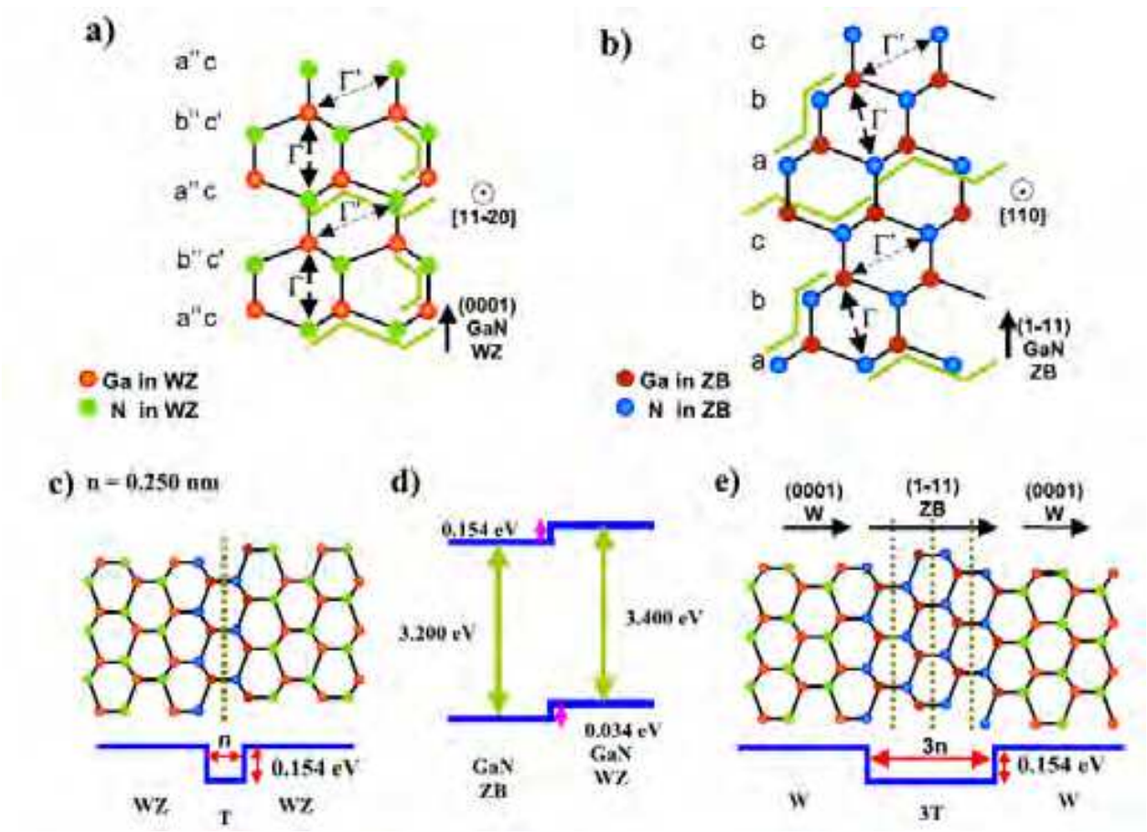

Fig. 4. Twin formation scheme

2.5 Local optical properties addressed through EELS: Plasmon position and structural considerations

Low-loss spectra were acquired along the doped NWs using a GIF2001 spectrometer coupled to a JEM2010F microscope. The plasmon position was found to remain constant along the NW. Now, the plasmon position depends on bandgap, but it also depends on other factors that may cancel out. In particular, it is possible to assume that plasmon position depends on the composition and the distance to the first neighboring atom, which are the same for WZ and ZB regions in the NWs, so that even if the bandgap changes, the plasmon energy remains the same. In other words, the unchanging plasmon position does not need to correspond to unchanging bandgap energy. This affirmation will be further sustained by ab-initio simulations in the following section. On the other hand, it is clear that EELS spectra with a better energy resolution are needed to access the bandgap energy.

Bandgap estimation

Aberration-corrected STEM, and EELS spectra with a 0.3 energy resolution were used to move one step further and locally analyze the local density of states at the atomic scale that

occur in the interface between the triple-twin (3T) planes (ZB) and the WZ GaN heterostructure. Experiments were performed on a dedicated VG HB 501 STEM retrofitted with a Nion quadrupole–octupole corrector (SuperSTEM 1) at Daresbury (Arbiol et al., 2009). Cs-corrected HRHAADF STEM micrographs, where the displayed bright spots directly correspond to the actual atomic positions, corroborate the proposed structural model for the 3T domains (Fig. 5. High-resolution HAADF twin domain and local HREELS Bandgap analysis). EEL spectra maps of the NWs were obtained with a zero loss peak (ZLP) energy FWHM of 0.3 eV and a probe size of about 0.1 nm. The much reduced probe size allowed us to obtain several EEL spectra in the direction perpendicular to the NW growth direction for wurtzite and 3T planes (see square blue and red marks in Fig. 5.(a) for the EELS selected areas). Then, the spectra obtained at the exact atomic positions with respect to the wurtzite and the 3T regions were processed and analyzed. These spectra are displayed in Fig. 5.(b). It is generally accepted that the ZLP shape is Gaussian (Egerton, 1996), and thus that it contributes to the low-loss signal as $A \exp(-rx^2)$, where x is the energy loss. In the present work, it was subtracted from the low-loss region by fitting an $A \exp(-rx^2)$ function to the positive tail of the ZLP. The resulting spectra (Fig. 5.(b)) show several interesting features –before analyzing the low-loss spectra, it should yet be noticed that the peak observed at about 24 eV is in fact the Ga 3d transition. The obtained band gap is found to be higher for the WZ region (measured to be 3.4 eV) than for the 3T region (measured to be 3.2 eV). The values are comparable to the band gap measurements for WZ and ZB phases obtained by EELS in literature (Bangert et al., 1998; Lazar et al., 2003) but, interestingly, lower than the values obtained using other techniques. On the other hand, features B and C in Fig. 5.(b) are found at higher energies for zinc-blende GaN than for wurtzite GaN. These peaks were expected, from first principles calculations (Gavrilenko & Wu, 2000), to arise from transitions from the three upper valence bands to the third and fourth conduction bands (B), and from the same bands to the fifth and upper conduction bands (C), occurring at higher energies for ZB GaN than for WZ GaN. Finally, the higher intensity of the EELS spectrum in the region <15 eV and the broadening of the plasmon peak for the faulty region can be related to the occurrence of surface modes (Egerton, 1996; Erni & Browning, 2005) corresponding to the WZ–ZB–WZ interface (Fig. 5.(b)). Specific ab initio simulations of the EELS spectra of pristine bulk wurtzite and defective bulk wurtzite (triply-twinned inclusion) were carried out (Figs. 5.(c) & (e)) in order to corroborate the origin of these experimental features. Ab initio calculations were carried out using the SIESTA (Soler et al., 2002) code, which combines density functional theory (DFT), normconserving pseudopotentials, and local basis set functions.

We used the generalized gradient approximations (GGAs) with the Perdew, Burke, and Ernzerhof (PBE) parameterization (Perdew et al., 1996). For Ga and N atoms, the double ζ local basis set was used with polarization. Additional d-electrons were included in the valence electron set of Ga. Well converged spectra were obtained with a real space mesh cut-off of 250 Ryd and Monkhorst–Pack sets larger than 34 × 34 × 18 for wurtzite structures. Experimental HRTEM lattice parameters were used to build all crystal models. Atomic positions were determined by performing structural relaxations using conjugate gradient minimization of the energy, until the forces on all the atoms were smaller than 0.04 eV Å−2. In the relaxation of the models, lattice dimensions were kept constant (in accordance with the experimental values) and no constraints were imposed on the atomic positions within the supercell. To model the planar defects, defective inclusions were embedded in pristine bulk wurtzite. Eight [0001] layers of Ga–N dimers were used to separate the periodic images

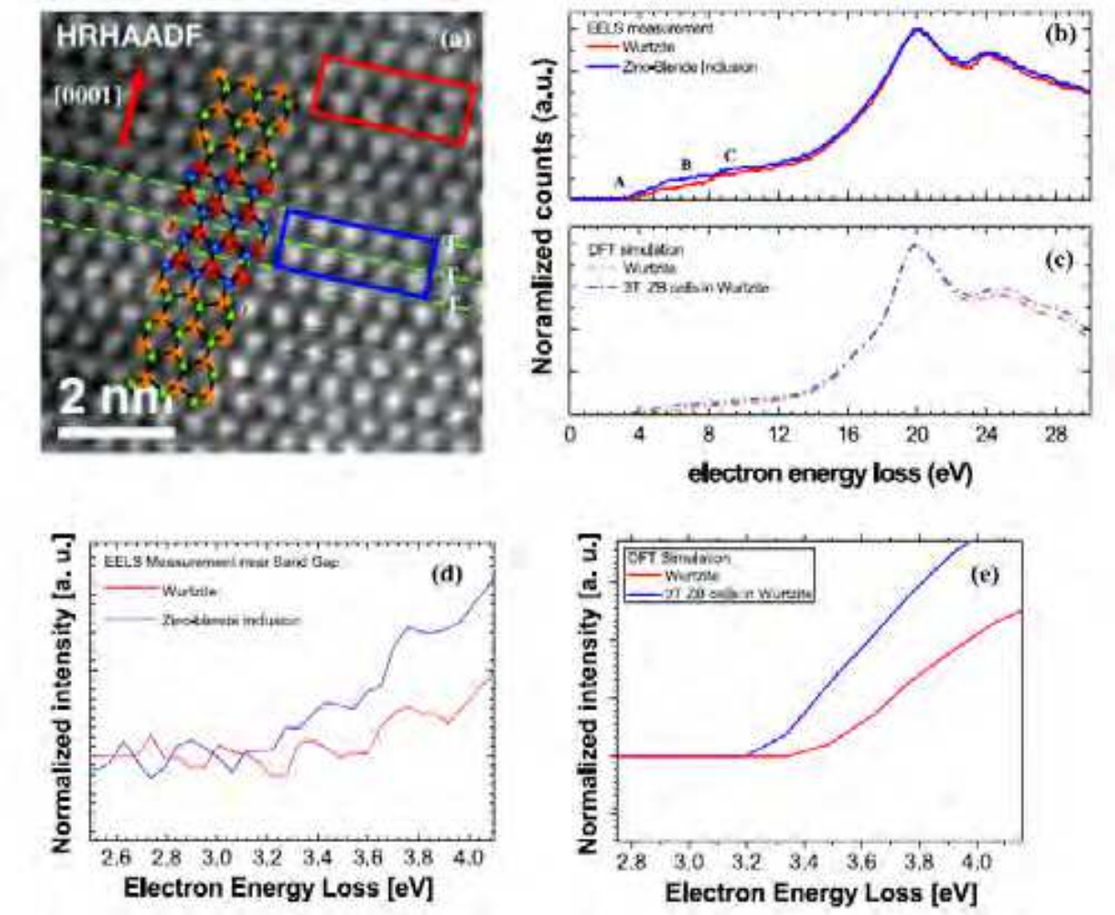

Fig. 5. High-resolution HAADF twin domain and local HREELS Bandgap analysis

of the defects. Variations in the electronic structure of less than 0.2% were observed for 16 spacing layers. The loss functions were obtained using first-order time-dependent perturbation theory to calculate the dipolar transition matrix elements between occupied and unoccupied single-electron eigenstates, as implemented in SIESTA 2.0. The optical matrix elements were calculated including the corrections due to the nonlocality of the pseudopotentials (Read & Needs, 1991), which were then used to obtain the dielectric function $\varepsilon(\omega)$ and the loss function $\mathrm{Im}\{-1/\varepsilon(\omega)\}$ that is directly comparable with the EELS spectra. It is well known that electronic structure calculations within DFT-GGA generally underestimate the band gap of semiconductors (Jones & Gunnarsson, 1989). In this case, the calculated band gap for the pristine wurtzite phase was EW g(GGA) = 2.42 eV, clearly lower than the experimental value EW g(exp) = (3.4 ± 0.1) eV. We followed the most common procedure in the literature to circumvent this difficulty that is to apply scissor operators (Levine & Allan, 1989; Hughes & Sipe, 1996) that rigidly shift the conduction band in order to match the position of the main peak of the calculated and experimental EELS spectra (located at 20.1 eV in Figs. 5.(b) & (c)). Figs. 5.(c) & (e) show the simulated spectrum of the pristine wurtzite bulk and the local spectrum of the 3T cells embedded in wurtzite. These calculations not only reproduce the main features (A, B, C in Fig. 5.(b)) of both situations but also predict the experimental band gap change (Figs. 5.(d) & (e)). Notice that all spectra have been normalized to the maximum of the plasmon peak in Figs. 5.(b) & (c).

3. 3D reconstruction of 1D complex nanostructures by means of electron tomography

3.1 State of the art

Tomography

Tomography is a technique used to reconstruct the 3D morphology of an object from its projecting images. The mathematical principles which allow these techniques were established since the theorem made by Radon in 1917 (Radon, 1917). However, the necessary computer tools were not developed enough in order to perform the complex calculations. The necessity to obtain higher dimension structures from data series of fewer proportions is present in many scientific fields. The first real application was made by Bracewell in the area of astronomy in 1956 (Bracewell, 1956). He proposed a method to recreate a 2D map related to the microwaves emission of sun from 1D fan beam series profiles measured with a microwave telescope. The usefulness of 3D reconstructions was confirmed by 2 Nobel Prizes. The first, in 1979, was given to A. Cormack (Cormack, 1980) and G.N Hounsfield (Hounsfield, 1980). They developed the Computerized Axial Tomography, a very well known diagnosis technique. The second Nobel Prize was given to Aaron Klug in 1982 (Klug, 1982). His work was pioneer in 3D reconstructions of molecular structures through projecting images obtained with electron microscopy. In nanoscience and nanotechnology it is very well known that the shape, size, and morphology of a nano-object are very important factors, sometimes with similar relevance than the material composition in the final physical and chemical behavior. Nanostructured materials like nanowires, for example, are becoming materials of a huge importance since its physical properties dissociate in a significant way from the behavior that the same material would have in bulk. In general, the effects due to the nanostructuration start from 1 to few hundred nanometers. Several experimental characterization techniques are able to obtain 3D information at nanometric scale. One example is the atom-probe-field-ion microscopy which can be applied to conductive samples used in mass spectrometry (Humphreys, 2007). Another example would be the serial sectioning approach in which a tridimensional model is reconstructed through a series of slices. From this, we can extract images trough cryo TEM or even with an Atomic Force Mircroscopy (AFM). The major problem of these cross-sectional techniques is that they are destructive. Moreover, image formation techniques based on magnetic resonance or X-ray absorption remind restricted outside the nanoscale. It is for this reason that Electron Tomography becomes a very important tool for the structural modeling of nanometric objects. Computerized tomography is directly related with Radon theorem. The Radon transform is defined as a mapping into the so-called Radon space of a function describing a real space object, by the projection, or line integral, through that function along all possible lines (Fig. 6. Radon transform scheme). The Radon transform R can be visualized as the integration through a body D in real space f(x,y) along all possible line integrals L, with its normal at an angle to the horizontal.

$$Rf = \int_L f(x,y)ds \tag{1}$$

Thus, given a sufficient number of projections, an inverse Radon transform of this space should reconstruct the object (Midgley & Weyland, 2003). A discrete sampling of the Radon transform is geometrically equivalent to the sampling of an experimental object by some form of transmitted signal or projection. The consequence of such equivalency is that the

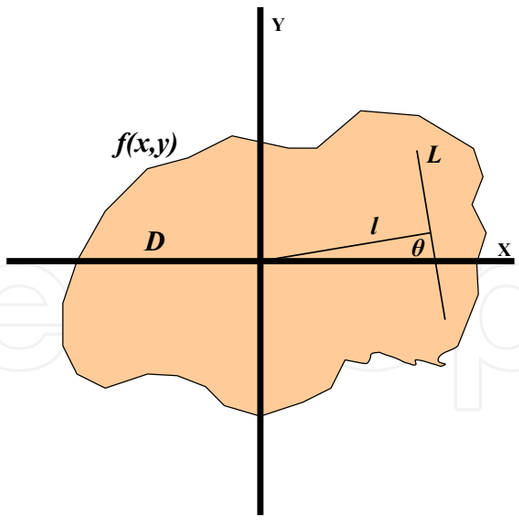

Fig. 6. Radon transform scheme

reconstruction of the structure of an object *f(x,y)* from projections *Rf* can be achieved by implementation of the inverse Radon Transform (Midgley & Weyland, 2003). In practice, the reconstruction that comes from projections is based on the knowledge between the relationship of the projections in the real space and Fourier space. The theorem of the central slice establishes that a projection of a given angle is a central section trough the Fourier transform of this object (Fig. 7. Sampling in Fourier space for tilting with equal increments). Thus, if a series of projections are acquired at different tilt angles, each projection will equate to part of an object's Fourier transform, sampling the object over the full range of frequencies in a central section.

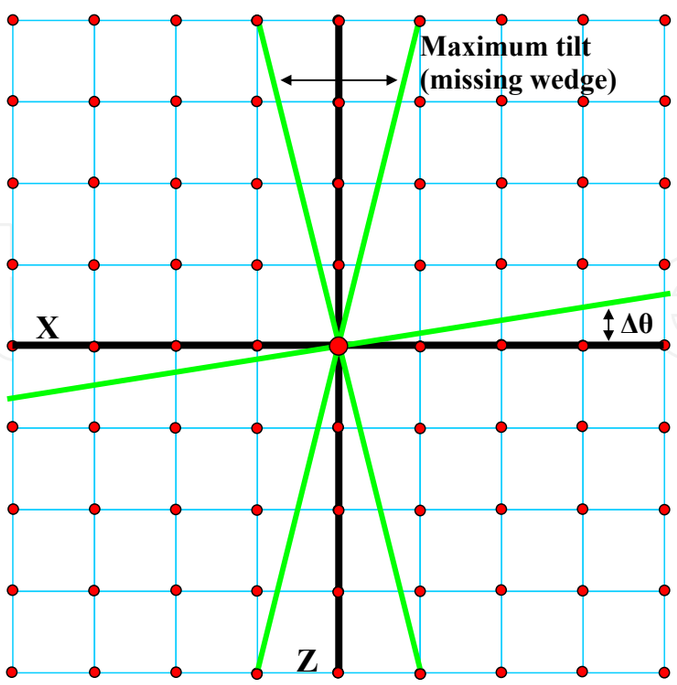

Fig. 7. Sampling in Fourier space for tilting with equal increments

Therefore tomographic reconstruction is possible from an inverse Fourier transform of the superposition of a set of Fourier transformed projections: an approach known as direct Fourier reconstruction. However, if projections are missing from an angular range, brought about by a limit on the maximum tilt angle, then Fourier space is under-sampled in those directions and as a consequence the back transform of the object will be degraded in the direction of this missing information. In this way, different sampling geometries, which are associated with the technical characteristics of the microscope sample holder and its capacity to fill the Fourier space can be used: single-axis, double-axis and conical (Penczek et al., 1995; Frank, 2006). Moreover, two problems appear in this formulation. Firstly, the projection data is always sampled at discrete angles leaving regular gaps in Fourier space. As the inverse transform requires a continuous function, radial interpolation is required to fill the gaps in Fourier space. Secondly, there is a non-uniform sampling of the data, which results in that the central zone of Fourier space has more information than the zones that are more remote. Thus, direct reconstruction methods have been replaced by the retroprojection method, which requires less compute power and allows to solve the problem of the inhomogeneities in the sampling in the Fourier space via application of some kind of filters, in general ramp filters: this method is know as Weighted BackProjection (WBP). The method of backprojection is based on inverting the set of recorded images, projecting each image back into an object space at the angle at which the original image was recorded. Using a sufficient number of backprojections, from different angles, the superposition of all the backprojected "slices" will reconstruct the original object. A schematic diagram of this approach is shown (Fig. 8. Scheme of 3D reconstruction via backprojection).

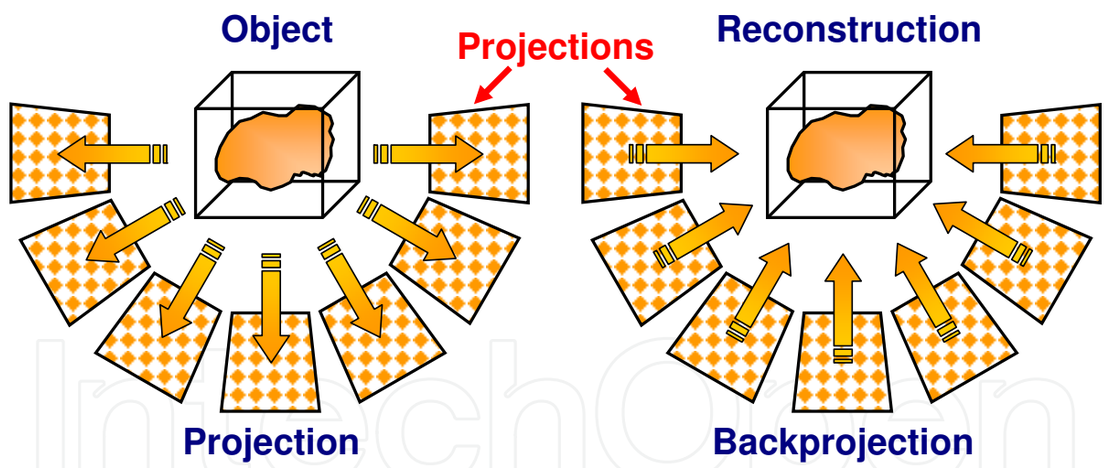

Fig. 8. Scheme of 3D reconstruction via backprojection. An object is sampled by projection from a range of angles and then reconstructed by backprojecting these projections at the original sampling angle into the object space

To provide maximum 3D information as many projections as possible should be acquired over as wide a tilt range as possible. Once we have introduced tomography fundamentals, we will focus our efforts on the electron tomography (Midgley & Weyland, 2003).

Electron tomography

The transmission electron microscope (TEM) is a very important tool in the structural and analytical characterization of objects at the nanoscale since it can offer us different sources of

information depending on the detectors that are used. However, most of the techniques that are associated with TEM are based on simple 2D projections obtained after the electron beam is transmitted through a 3D object. As it has been said before, in order to recover the tridimensional information lost with the projections we can apply some tomographic reconstruction techniques (Fig. 9. TEM tomography geometries). These techniques are widely used in the areas of medicine. Nevertheless, electronic tomography has been very little used in materials science basically for two major reasons: a) in general, inorganic materials have few 3D structure and they can be very well described by 2D projections; b) In contrast to the biology area or organic composites, tomography based on bright field (BF) images does not give accurate results as far as the crystalline samples are concerned (Weyland, 2002; Midgley et al., 2007). The explanation to this is that in order that a reconstruction can be faithful to the real object, the intensity of the projecting image must be a monotonous function of some characteristics of the real object. The amount of material projected in a parallel direction to electron beam could be a good example of this. This is known as a projection requirement. In crystalline samples, the contrast in BF conditions is ruled by the diffraction, which is related to the Bragg conditions and not necessary to the thickness of the material projected. Even all this, in the last years there has been a great effort to solve this problem by using the TEM operative mode High Angle Annular Dark Field (HAADF) (Koguchi et al., 2001; Midgley et al., 2001). Electrons scattered to low angles are predominantly coherent in nature and therefore, conventional BF and DF images exhibit sudden contrast changes depending on specimen thickness, orientation or defocus. This observation mode feature does not obey the projection requirement.

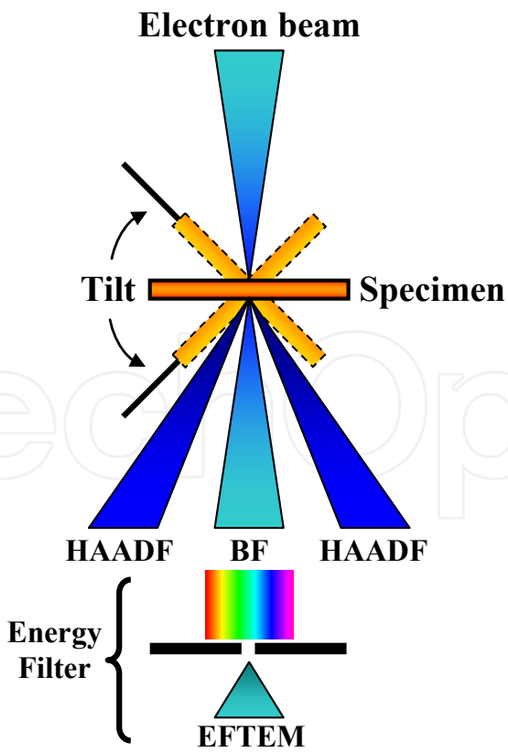

Fig. 9. Summary of the geometries of the various signals that may be used for tomographic reconstruction in TEM

However, electrons scattered to high angles are predominantly incoherent, and images formed using HAADF detector do not show the contrast changes associated with coherent scattering. Such high angle scattering is associated with electron interaction close to the nucleus of the atom and thus the cross-section for HAADF scattering approaches the unscreened Rutherford cross-section, which is strongly dependent on the atomic number Z. In practice the unscreened limit is never reached and the exact dependence depends on many factors. Nevertheless, medium-resolution STEM images formed with a HAADF detector are very sensitive to changes in specimen composition with the intensity varying monotonically with composition and specimen thickness, thus satisfying the projection requirement and giving an extra information on sample composition as it is possible to discern between different materials composing the studied reconstructed structure. For a comparison between the results obtained in crystalline samples by BF-TEM and HAADF-TEM see (Fiedrich et al., 2005). On one hand, it must be said that if HAADF gives the chance to obtain 3D structural reconstructions of crystalline nanostructures, while the Energy Filtered TEM (Möbus et al., 2003) and Electron Energy Loss Spectroscopy (van den Broek et al., 2006) have demonstrated to be a valid tool in order to find 3D compositional maps of nanostructured materials. On the other hand, the combination of HAADF with the Scanning TEM mode shows a great advantage since in scanning mode the electron dose on the surface area is time limited and then the sample damage is reduced. In the last years electron tomography has been applied to obtain solve 3D morphological and compositional problems related to nanowire synthesis. Up to our knowledge the first time that electron tomography was applied on NWs, was in 2004 to discern the growth of Metal Nanowires (Pt) inside hard template mesoporous silica (Arbiol et al., 2004a; Arbiol et al., 2004b). Lately, and thanks to the development of the HAADF STEM tomography technique, application of electron tomography to crystalline nanostructures such as nanowires has been extended. In this way, it has been applied for example to analyze the 3D morphology of core-shell GaP-GaAs NWs (Verheijen et al., 2007), the 3D structure of helical and zigzagged nanowires (Kim et al., 2008), the microsctructure of magnetic $CoFe_2O_4$ nanowires inside carbon nanotubes (Ersen et al., 2008), the 3D surface defects in core-shell nanowires (Arslan et al., 2008), the homogeneity of prismatic heterostructures on the facets of catalyst-free GaAs nanowires (Heigoldt et al., 2009), the 3D chemical arrangement on Ge-Si Nanostructures (Montoro et al., 2009) or the 3D line edge roughness in Cu NWs (Ercius et al., 2009).

3.2 Particular case: HAADF STEM tomography of coaxial multi-quantum wells in semiconductor nanowires

In order to demonstrate the capabilities of the Electron Tomography as characterization tool in the field of inorganic nanostructured crystalline materials, we have applied STEM-HAADF Tomography to coaxial nanowire heterostructures with variable quantum well thickness. In recent times the interest in III-V semiconductor nanowires has received renewed attention due to their applications in electronics and optoelectronics. The improvements of new methods of synthesis and characterization, has turned nanowires (and other nanostructures) into testers of quantum-mechanical effects (Hu et al., 2007; Shorubalko et al., 2008; Heigoldt et al., 2009). More complex structures have been obtained by combining materials coaxially and axially along the growth direction of the nanowires. Up to now, coaxial heterostructures have been considered to improve the performance of nanowire devices to confine the carriers at the core, leading to the reduction of surface

scattering (Wang et al., 2005). Core-shell structures have also been used for engineering the optoelectronical properties of the core, for example for the fabrication of multi-color light emitting diodes or lasers (Quian et al., 2008). Little attention has been paid to the geometry of the deposited shell, as the main functionality continued to be reserved to the core of the nanowire. Recently, we have shown that is possible to uniformly coat the nanowires with successive epitaxial layers resulting into multiple quantum heterostructures defining for example prismatic quantum wells (p-QW) (Morral et al., 2008b). Growth of p-QWs constitutes an additional functionality to the nanowire and, accordingly, an increased freedom design for nanostructures and devices. As a result, new architectures based in coaxial heterostructures (Fig. 10. HRTEM transversal section of AlAs-GaAs MQW nanowires grown on (001) and (111)B GaAs substrates) are being synthesized and investigated, due to their optoelectronic properties and consequent applications in the fabrication of light-emitting diodes (LEDs). Compared to bulk samples, where electrons and holes can propagate in all three dimensions, there are new effects emerging when this is no longer the case. By introducing potential barriers for these carriers one can confine them in one, two or three spatial directions. If the dimension of the confinement is of the order of the Fermi wavelength, this results into quantum confinement, ending up with carriers which can only propagate freely in less than three dimensions, speaking then of quantum wells (2D), wires (1D) or dots (0D) respectively (Wegscheider et al., 1993; Schedelbeck et al., 1997). In the example selected to illustrate the electron tomography potentiality, we used a layer sequence of $Al_{0.35}Ga_{0.55}As$, GaAs, $Al_{0.35}Ga_{0.55}As$ for building the quantum well and a final layer of GaAs to prevent oxidation of $Al_{0.35}Ga_{0.55}As$.

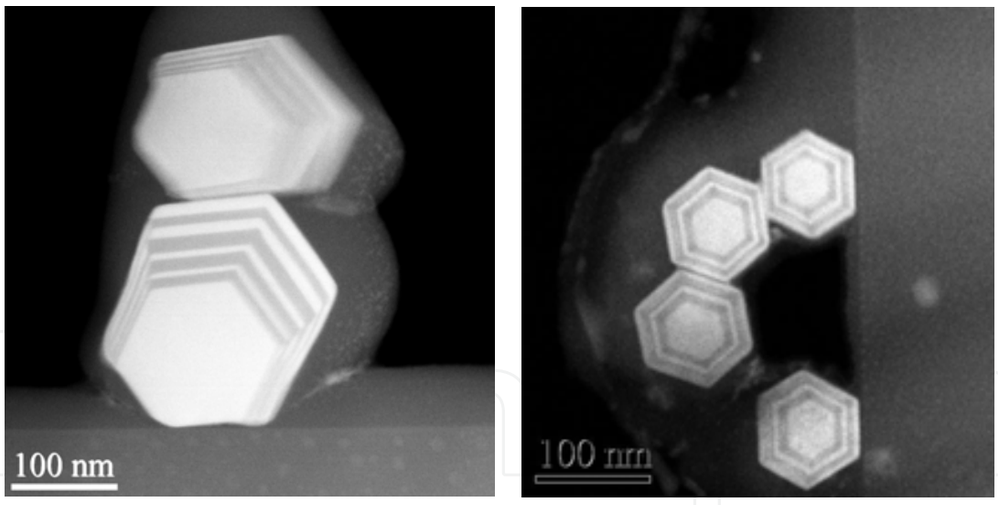

Fig. 10. HRTEM transversal section of AlAs-GaAs MQW nanowires grown on (001) and (111)B GaAs substrates, left and right, respectively

For this material combination, a type I quantum well is formed in the GaAs layer sandwiched between the $Al_{0.35}Ga_{0.55}As$ barrier layers. By varying the thickness of the QW, it is possible to control the confinement energy of the carriers. In this way the wavelength of the emitted light can be tuned, adding new functionality to the heterostructured NWs. Nanowires have been grown on a (001) and (111)B GaAs substrates by molecular beam epitaxy (MBE). The substrate was coated with a SiO_2 layer of about 10nm thick. A recent work (Morral et al., 2008a) showed that when the thickness of SiO_2 is less than 30nm an

epitaxial growth of the nanowire with respect to the substrate exists, thanks to the penetration of the Ga catalyst through nanometric pinholes allowing the contact between substrate and wire. By changing the growth conditions, it is possible to switch between nanowire axial growth and typical MBE planar growth. This results in the possibility of depositing layers in an epitaxial way on the nanowire facets. Then, due to the directionality of the molecular beam, the thickness of the layers will depend if the nanowire is standing perpendicular to the substrate or with an angle (Heigoldt et al., 2009). A scheme of the epitaxial growth on the nanowire facets and the respective band alignement of quantum wells grown on the facets, depending on substrate orientation is shown in Fig. 11. As [111]B growth axis is the preferentially followed by the nanowires (Morral et al., 2008a), the growth of the epitaxed nanowire over the (001) GaAs substrate leads to a non perpendicular orientation of the nanowire (35º leaning with respect to the substrate), implying a inhomogeneous configuration of the coating over the different faces of the hexagonal nucleus with quantum wells of distinct thickness in each lateral side. Oppositely, those nanowires grown on [111]B substrates, would be oriented perpendicularly to the substrate, thus implying a homogeneous shell covering on all the lateral facets.

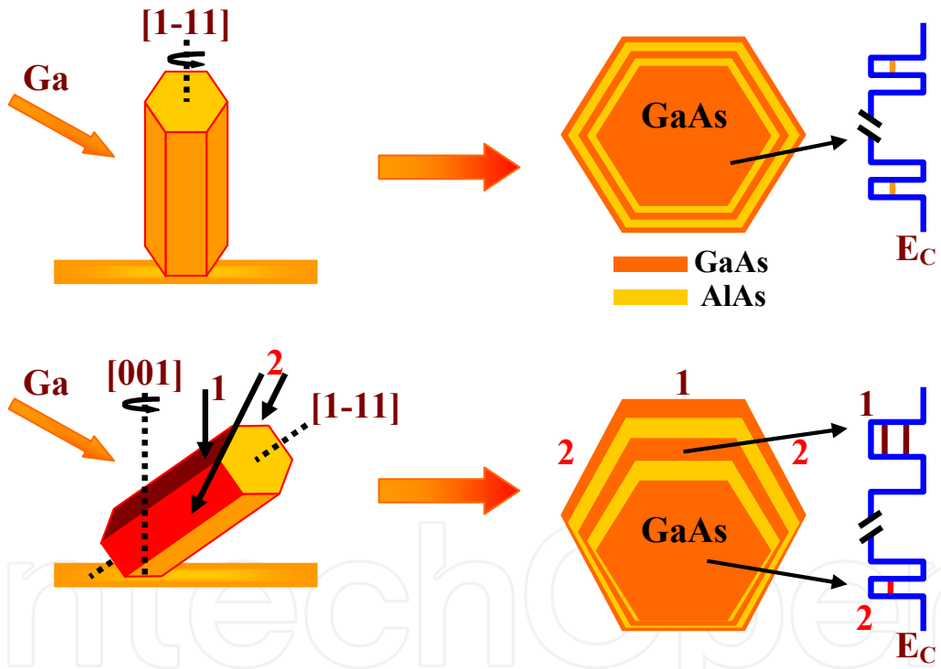

Fig. 11. Scheme of Nanowires growth and band alignment of quantum wells grown epitaxially on the facets depending on substrate orientation

As a consequence, several emission peaks in photoluminescence (PL) are observed, depending on the nanowire configuration on the substrate. This is in good agreement with the proposed scheme. (Morral et al., 2008b). In the case where six identical quantum well-like states exists, one would expect other confinement states at the six corners where the QWs cross. Due to the effectively increased distance between the barriers in such a corner, i.e. the wavefunctions of electrons and holes should be less confined than in a QW, forming a one dimensional quantum wire like state, as shown in previous calculations (Heigoldt et

al., 2009). Such states have already been demonstrated experimentally at the intersection of two quantum wells, using for example the technique of cleaved edge overgrowth or by overgrowth of so call V-grooves (Kaufman et al., 1999; Merano et al., 2006). The distance in energy of such a one dimensional state to the ground state in the QWs is small, usually in the order of meV, demanding a very good homogeneity of the QW width, in order to be resolved experimentally by photoluminescence (Wegscheider et al., 1994; Wegscheider et al., 1999).

3.3 HAADF STEM tomography

In order to carry out this experimental approach we have used a TEM JEOL 2100 with a HAADF detector. To obtain the data we used the GATAN 3D Tomography-Acquisition Software as well as the 3D Reconstruction and 3D Visualization PlugIns integrated in the well-known Digital Micrograph package. The microscope holder used was an EM-21010/21311 HTR-High Tilt Holder, specially designed to allow a high tilt performance up to ± 80º. This software is able to account for the acquisition, image processing and electron energy loss spectroscopy (EELS) tools to quantitatively extract structural and chemical information of the sample. Since the samples object of the present research were of crystalline nature, we used STEM-HAADF mode for the development of tomography. In all the reconstructions made in the present work we have followed 3D Simultaneous Iterative Reconstruction Technique (SIRT) by plane, which consists in multiple iteration algorithms to try to minimize errors in the reconstruction that arise from the reconstruction process. These techniques have been useful for minimizing the effect of incomplete tilt range coverage commonly referred to at the "missing wedge". The number of iterations has been 15 since the results we obtained were successful. Complete tomographic reconstruction movies related to the samples analyzed will be available in the following web site: http://www.icmab.cat/gaen

3D reconstruction model of the MQW NWs grown on (001) substrates

A series of AlAs and GaAs layers of thicknesses ranging from 8 to 30 nm was grown on inclined wires, as grown on (001) GaAs substrates. As schematized in Fig. 11., in this case where the NWs are oriented with an angle of 35º with respect to the surface, the flux of adatoms is different for each of the six nanowire sidewalls. The top facets are facing the flux and therefore the thickness of their grown layers should be the thickest.

As it can be observed in Fig. 10. (left), this is also what it is observed from the cross-section HAADF (S)TEM analysis. The growth rate on the other facets is smaller, with the facets facing the substrate surface showing almost no growth. A 3D HAADF Tomography reconstruction of a p-QW NW grown on (001) GaAs substrate has been also obtained in order to verify the 3D geometrical configuration. For this purpose we selected a NW grown on a (001) GaAs substrate and obtained the corresponding tilt series on HAADF. The 3D tomographic reconstruction is shown (Fig. 12. 3D tomographic reconstruction of the multiwalled nanowire nature and the inhomogeneous layer thickness), where we can appreciate that the difference in thickness of the various facets of the NW. The tomographic reconstruction has been made from the series of images taken at the top end of the nanowire which at -28º has a diameter of 235 nm, and with projections from -72º to +56º, eventhough the last 10 projections were removed because of pollution problems. In order to remove the shift 23 iterations have been made. The core of the nanowire (GaAs) has a diameter of 128

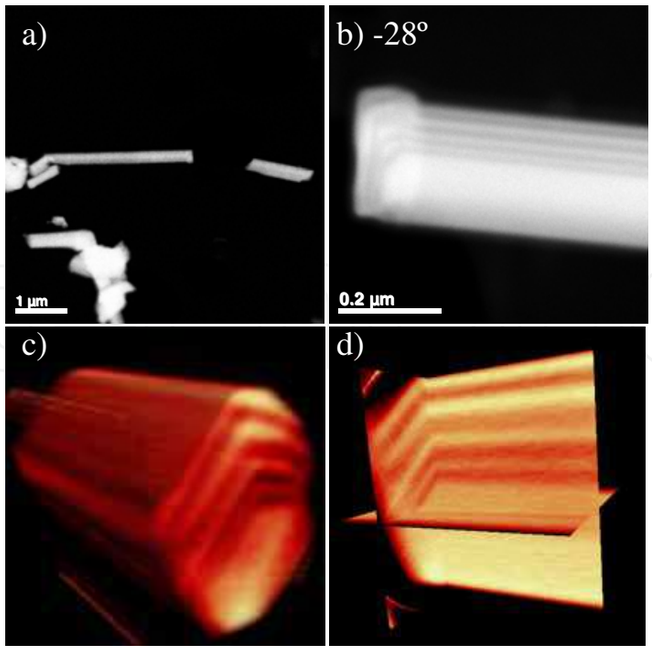

Fig. 12. a) general view of the characterized nanowire. b) HAADF image at -28º tilt (the presence of multiple shells is observed). c) Volumetric reconstruction of the nanowire. d) Ortho slices in the tomographic reconstruction that show the multiwalled nanowire nature and the inhomogeneous layer thickness.

nm and the nanowire presents four coatings of successive layers of AlAs and GaAs, respectively. The AlAs layers increase their width between 10 nm to 15 nm and the GaAs between 11 nm to 19 nm, in radial direction. Finally, the 3D reconstruction allows obtaining additional information which was not possible in the case of a cross section. Indeed, we observe that the QWs on individual facets are of equal thickness along the nanowire facet, indicating a homogeneous epitaxial growth along the whole nanowire. This is in agreement with the homogeneity of the optical properties along the nanowire axis, as reported elsewhere (Heigoldt et al., 2009).

3D reconstruction model of the MQW NWs grown on (111)B substrates

In the case of those NWs grown on (111)B GaAs substrates, we expect a homogeneous coaxial structure in all of the facets, as schematized in Fig. 11 and observed in Fig. 10. (right), from the cross-section HAADF (S)TEM analysis.

As in the previous case, the complete tomographic reconstruction of one of these NWs was obtained in order to assure the perfect homogeneity of the p-QW within the 6 facets and along the NW. For this purpose we obtained the tilt series on the same area shown in Fig. 10. (right). In Fig. 13. the 3D reconstruction of the sectioned NWs shown in Fig. 10. (right) has been obtained. From these measurements we find that the quantum wells are flat and homogeneous in thickness along the whole nanowire in good agreement with the previous HRTEM results. Thicknesses measured on the 3D reconstruction are in good agreement with those obtained earlier by cross-sectional HAADF STEM. However, thanks to the 3D reconstruction, we can assure that the measured thicknesses are kept along the whole NW growth axis. Not surprisingly, it is found again that the scaling factor, e.g. the quotient of the

measured and the nominal thickness is approximately constant for the AlAs layers. This means that diffusion from the substrate to the facets of the NW plays a minor role on the deposition mechanisms on the facets.

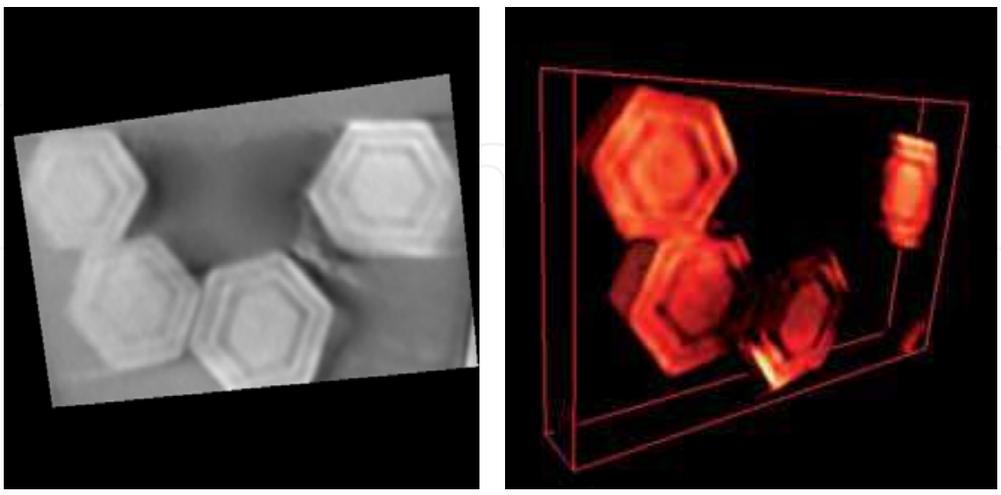

Fig. 13. Tomography slice obtained from the reconstructed 3D volume (left). 3D reconstructed model of several NWs with homogeneous MQWs.

4. Conclusion

In the present chapter we have shown how advanced tools in electron nanoscopy can help analyze complex nanostructured nanowires. On one hand, EELS combined with STEM has been applied to characterize the features produced by the Mg doping in GaN nanowires grown by plasma assisted molecular beam epitaxy to obtain p-type nanostructures and their effects on the nanowire. As observed by (S)TEM, the presence of Mg results in the formation of triple-twin (3T) defects, which increase with increasing Mg concentration. The high concentration of misplaced atoms gives rise to local changes in the crystal structure equivalent to three non-relaxed atomic cells of zinc-blende (ZB), which define quantum wells (QW) along the wurtzite (WZ) nanowire growth axis. Local EEL spectra obtained on the 3T and wurtzite planes show modifications in the local density of states, in which the band to band electronic transition energies change from 3.4 eV (for the wurtzite band gap) to 3.2 eV in the 3T lattice regions, the latter being in good agreement with the band gap measured in GaN ZB structures by EELS. These results are confirmed by specific ab initio atomistic simulations of these two situations. EELS assessment of the optoelectronic properties of the given nanostructures at a subnanometric scale has been successfully demonstrated. On the other hand, we have shown how Z-contrast or HAADF electron tomography is a perfect tool in order to characterize the morphology of complex heterostructures in nanowires. We have presented the implementation and optimization of the tomographic methods in electron microscopy and its best performance for NW applications. These methods have been tested to carry out tomographic reconstruction of several coaxial core-shell heterostructures in semiconductor nanowires, in order to obtain their corresponding 3D information. This last promising 3D technique allowed a better understanding of the structure of our coaxial nanowires and is an excellent complement to the high resolution cross-sectional imaging modes.

5. Acknowledgements

We kindly acknowledge Prof. Anna Fontcuberta i Morral groups from EPFL (Lausanne, Switzerland) and WSI-TUM (Garching, Germany) for the synthesis of GaAs multiquantum-well nanowires used in electron tomography analyses examples, as well as for her contribution and discussions on the present chapter. We also want to acknowledge Prof. Martin Eickhoff groups in WSI-TUM (Garching, Germany) and Justus-Liebig-Universität (Giessen, Germany) for the synthesis of Mg doped GaN nanowires used to illustrate advances in EEL spectroscopy applied to Nanowires. We also want to thank Serveis Cientificotècnics of Universitat de Barcelona for the use of their TEM facilities (Barcelona, Spain).

6. References

Algra, R. E.; Verheijen, M. A.; Borgstrom, M. T.; Feiner, L-F.; Immink, G.; van Enckevort, W. J. P.; Vlieg, E. & Bakkers, E. P. A. M. (2008). Twinning superlattices in indium phosphide nanowires. *Nature*, 456, 7220, (November 2008) 369-372, ISSN: 0028-0836

Allen, J. L.; Findlay, S. D.; Lupini, A. R.; Oxley, M. P. & Pennycook, S. J. (2003). Atomic-resolution electron energy loss spectroscopy imaging in aberration corrected scanning transmission electron microscopy. *Physical Review Letters*, 91, 10, (September 2003) 105503, ISSN: 0031-9007

Appenzeller, J.; Knoch, J.; Bjork, M. T.; Riel, H.; Schmid, H. & Riess, W. (2008). Toward nanowire electronics. *IEEE Transactions on electron devices*, 55, 11, (November 2008) 2827-2845, ISSN: 0018-9383

Arbiol, J.; Cirera, A.; Peiró, F.; Cornet, A.; Morante, J. R.; Delgado, J. J. & Calvino, J. J. (2002). Optimization of tin dioxide nanosticks faceting for the improvement of palladium nanocluster epitaxy. *Applied Physics Letters*, 80, 2, (January 2002) 329-331, ISSN: 0003-6951

Arbiol, J.; Rossinyol, E.; Cabot, A.; Peiro, F.; Cornet, A.; Morante, J. R.; Chen, F. L. & Liu, M. L. (2004). Noble metal nanostructures synthesized inside mesoporous nanotemplate pores. *Electrochemical and Solid State Letters*, 7, 7, (January 2004) J17-J19, ISSN: 1099-0062

Arbiol, J.; Rossinyol, E.; Cabot, A.; Peiro, F.; Cornet, A. & Morante, J. R. (2004). TEM 3D tomography of noble metal nanowires growth inside SiO2 mesoporous aggregates. *Materials Research Society Symposium Proceedings*, 818, (April 2004) 61-65, ISSN: 0272-9172

Arbiol, J.; Kalache, B.; Roca i Cabarrocas, P.; Morante, J. R. & Morral, A. F. I. (2007). Influence of Cu as a catalyst on the properties of silicon nanowires synthesized by the vapour-solid-solid mechanism. *Nanotechnology*, 18, 30, (August 2007) 305606, ISSN: 0957-4484

Arbiol, J.; Comini, E.; Faglia, G.; Sberveglieri, G. & Morante, J. R. (2008). Orthorhombic Pbcn SnO2 nanowires for gas sensing applications. *Journal of Crystal Growth*, 310, 1, (January 2008) 253-260, ISSN: 0022-0248

Arbiol, J.; Morral, A. F. I.; Estradé, S.; Peiró, F.; Kalache, B.; Roca i Cabarrocas, P. & Morante, J. R. (2008). Influence of the (111) twinning on the formation of diamond cubic/diamond hexagonal heterostructures in Cu-catalyzed Si nanowires. *Journal of Applied Physics*, 104, 6, (September 2008) 064312, ISSN: 0021-8979

Arbiol, J. ; Estrade, S. ; Prades, J. D. ; Cirera, A. ; Furtmayr, F. ; Stark, C. ; Laufer, A. ; Stutzmann, M. ; Eickhoff, M. ; Gass, M. H. ; Bleloch, A. L. ; Peiro, F. & Morante. J. R. (2009). Triple-twin domains in Mg doped GaN wurtzite nanowires: structural and electronic properties of this zinc-blende-like stacking. *Nanotechnology*, 20, 14, (April 2009) 145704, ISSN : 0957-4484; Fig. 3.(c) Reprinted with permission from this paper. Copyright [2008], American Institute of Physics.

Arenal, R.; Stéphan, O.; Kociak, M.; Taverna, D.; Loiseau, A. & Colliex, C. (2008). Optical gap measurements on individual boron nitride nanotubes by electron energy loss spectroscopy. *Microscopy and Microanalysis*, 14, 3, (June 2008) 274-282, ISSN: 1431-9276

Arslan, I.; Talin, A. A. & Wang, G. T. (2008). Three-dimensional visualization of surface defects in core-shell nanowires. *Journal of Physical Chemistry C*, 112, 30, (July 2008) 11093-11097, ISSN: 1932-7447

Banerjee, R.; Bhattacharya, A.; Genc, A. & Arora, B. M. (2006). Structure of twins in GaAs nanowires grown by the vapour-liquid-solid process. *Philosophical Magazine Letters*, 86, 12, (December 2006) 807-816, ISSN: 0950-0839

Bangert, U.; Harvey, A.; Davidson, J.; Keyse, R. & Dieker, C. (1998). Correlation between microstructure and localized band gap of GaN grown on SiC. *Journal of Applied Physics*, 83, 12, (June 1998), 7726-7729, ISSN: 0021-8979

Bao, J.; Bell, D. C.; Capasso, F.; Wagner, J. B.; Martensson, T.; Trägardh, J. & Samuelson, L. (2008). Optical properties of rotationally twinned InP nanowire heterostructures. *Nanoletters*, 8, 3, (March 2008) 836-841, ISSN: 1530-6984

Batson, P. E.; Kavanah, K. L.; Woodall, J. M. & Mayer, J. M. (1986). Electron-energy-loss scattering near a single misfit dislocation at the gaas/gainas interface. *Physical Review Letters*, 57, 21, (November 1986) 2729-2732, ISSN: 0031-9007

Batson, P. E.; Dellby, N. & Krivanek, O. L. (2002). Sub-angstrom resolution using aberration corrected electron optics. *Nature*, 418, 6898, (August 2002) 617-620, ISSN: 0028-0836

Boukai, A. I.; Bunimovich, Y.; Tahir-Kheli, J.; Yu, J. K.; Goddard, W. A. & Heath, J. R. (2008). Silicon nanowires as efficient thermoelectric materials. *Nature*, 451, 7175, (January 2008) 168-171, ISSN: 0028-0836

Bracewell, R. N. (1956). Two dimensional aerial smoothing in radio astronomy. *Australian Journal of Physics*, 9, 3, (January 1956) 297-314, ISSN: 0004-9506

Calleja, E.; Sánchez-García, M. A.; Sánchez, F. J.; Calle, F.; Naranjo, F. B.; Muñoz, E.; Jahn, U. & Ploog, K. (2000). Luminescence properties and defects in GaN nanocolumns grown by molecular beam epitaxy. *Physical Review B*, 62, 24, (December 2000) 16826-16834, ISSN : 1098-0121

Calvert, C. C.; Brown, A. & Brydson, R. (2005). Determination of the local chemistry of iron in inorganic and organic materials. *Journal of Electron Spectroscopy and Related Phenomena*, 143, 2-3, (May 2005) 173-187, ISSN: 0368-2048

Chen, C-C.; Yeh, C-C.; Chen, C-H.; Yu, M-Y.; Liu, H-L.; Wu. J-J.; Chen, K-H.; Chen, L-C.; Peng, J-Y. & Chen, Y-F. (2001). Catalytic growth and characterization of gallium nitride nanowires. *Journal of the American Chemical Society*, 123, 12, (March 2001) 2791-2798, ISSN: 0002-7863

Cheng, G. S.; Kolmakov, A.; Zhang, Y.; Moskovits, M.; Munden, R.; Reed, M. A.; Wang, G.; Moses, D. & Zhang, J. (2003). Current rectification in a single GaN nanowire with a

well-defined p-n junction. *Applied Physics Letters*, 83, 8, (August 2003) 1578-1580, ISSN: 0003-6951

Cimpoiasu, E.; Stern, E.; Klie, R.; Munden, R. A.; Cheng, G. & Reed, M. A. (2006). The effect of Mg doping on GaN nanowires. *Nanotechnology*, 17, 23, (December 2006) 5735-5739, ISSN: 0957-4484

Colliex, C. (1991). The impact of EELS in materials science. *Microscopy Microanalysis and Microstructures*, 2, 2-3, (April-June 1991) 403-411, ISSN: 1154-2799

Colombo, C.; Spirkoska, D.; Frimmer, M.; Abstreiter, G. & Morral, A. F. I. (2008). Ga-assisted catalyst-free growth mechanism of GaAs nanowires by molecular beam epitaxy. *Physical Review B*, 77, 15, (April 2008) 155326, ISSN: 1098-0121

Colombo, C.; Heiβ, M.; Gratzel, M. & Morral, A. F. I. (2009). Gallium arsenide p-i-n radial structures for photovoltaic applications. *Applied Physics Letterrs*, 94, 17, (April 2009) 173108, ISSN: 0003-6951

Cormack, A. M. (1980). Early two-dimensional reconstruction and recent topics stemming from it. *Science*, 209, 4464, (September 1980) 1482-1486, ISSN: 0036-8075

Davidson, F. M.; Lee, D. C.; Fanfair, D. D. & Korgel, B. A. (2007). Lamellar twinning in semiconductor nanowires. *Journal of Physical Chemistry C*, 111, 7, (February 2007) 2929-2935, ISSN: 1932-7447

De Franceschi, S.; van Dam, J. A.; Bakkers, E. P. A. M.; Feiner, L. F.; Gurevich, L. & Kouwenhoven, L. P. (2003). Single-electron tunneling in InP nanowires. *Applied Physics Letterrs*, 83, 2, (July 2003) 344-346, ISSN: 0003-6951

Egerton, R. F. (1996). *Electron Energy Loss in the Electron Microscope (2nd ed.)*, Plenum Press, ISBN-10: 0-306-45223-5 , New York

Egerton, R. F. (2003). New techniques in electron energy-loss spectroscopy and energy-filtered imaging. *Micron*, 34, 3-5, (August 2002) 127-139, ISSN: 0968-4328

Ercius, P.; Gignac, L. M.; Hu, C. K. & Muller, D. A. (2009). Three-Dimensional Measurement of Line Edge Roughness in Copper Wires Using Electron Tomography. *Microscopy and Microanalysis*, 15, 3, (June 2009) 244-250, ISSN: 1431-9276

Erni, R. & Browning, N. D. (2005). Valence electron energy-loss spectroscopy in monochromated scanning transmission electron microscopy. *Ultramicroscopy*, 104, 3-4, (October 2005) 176-192, ISSN: 0304-3991

Ersen, O.; Begin, S.; Houlle, M.; Amadou, J.; Janowska, I.; Greneche, J. M.; Crucifix, C. & Pham-Huu, C. (2008). Microstructural investigation of magnetic CoFe2O4 nanowires inside carbon nanotubes by electron tomography. *Nano Letters*, 8, 4, (April 2008) 1033-1040, ISSN: 1530-6984

Fischer, S. F.; Apetrii, G.; Kunze, U.; Schuh, D. & Abstreiter, G. (2006). Energy spectroscopy of controlled coupled quantum-wire states. *Nature Physics*, 2, 2, (February 2006) 91-96, ISSN: 1745-2473

Friedrich, H.; McCartney, M. R. & Buseck, P. R. (2005). Comparision of intensity distributions in tomograms from BF TEM, ADF STEM, HAADF STEM, and calculated tilt series. *Ultramicroscopy*, 106, 1, (December 2005) 18-27, ISSN: 0304-3991

Furtmayr, F.; Vielemeyer, M.; Stutzmann, M.; Arbiol, J.; Estradé, S.; Peirò, F.; Morante, J. R. & Eickhoff, M. (2008). Nucleation and growth of GaN nanorods on Si „111… surfaces by plasma-assisted molecular beam epitaxy - The influence of Si- and Mg-doping. *Journal of Applied Physics*, 104, 3, (August 2008) 034309, ISSN: 0021-8979

Furtmayr, F.; Vielemeyer, M.; Stutzmann, M.; Laufer, A.; Meyer, B. K. & Eickhoff, M. (2008). Optical properties of Si- and Mg-doped gallium nitride nanowires grown by plasma-assisted molecular beam epitaxy. *Journal of Applied Physics*, 104, 7, (October 2008) 074309, ISSN: 0021-8979

Gavrilenko, V. I. & Wu, R. Q. (2000). Energy loss spectra of group III nitrides. *Applied Physics Letters*, 77, 19, (November 2000) 3042-3044, ISSN: 0003-6951

Grogger, W.; Varela, M.; Ristau, R.; Schaffer, B.; Hoffer, F. & Krishnan, K. M.. (2005). Energy-filtering transmission electron microscopy on the nanometer length scale. *Journal of Electron Spectroscopy and Related Phenomena*, 143, 2-3, (May 2005) 139-147, ISSN: 0368-2048

Haider, M.; Uhlemann, S.; Schwan, E.; Rose, H.; Kabius, B. & Urban, K. (1998). Electron microscopy image enhanced. *Nature*, 392, 6678, (April 1998) 768-769, ISSN: 0028-0836

Heigoldt, M.; Arbiol, J.; Spirkoska, D.; Rebled, J. M.; Conesa-Boj, S.; Abstreiter, G.; Peiro, F.; Morante, J. R. & Morral, A. F. I. (2009). Long range epitaxial growth of prismatic heterostructures on the facets of catalyst-free GaAs nanowires. *Journal of Materials Chemistry*, 19, 7, (January 2009) 840-848, ISSN: 0959-9428

Hernandez-Ramirez, F.; Tarancon, A.; Casals, O.; Arbiol, J.; Romano-Rodriguez, A. & Morante, J. R. (2007). High response and stability in CO and humidity measures using a single SnO2 nanowire. *Sensors and Actuators B*, 121, 1, (January 2007) 3-17, ISSN: 0925-4005

Hochbaum, A. I.; Chen, R.; Diaz Delgado, R.; Liang, W.; Garnett, E. C.; Najarian, M.; Majumdar, A. & Yang , P. (2008). Enhanced thermoelectric performance of rough silicon nanowires. *Nature*, 451, 7175, (January 2008) 163-167, ISSN: 0028-0836

Hounsfield, G. N. (1980). Computed Medical Imaging. *Science*, 210, 4465, (October 1980) 22-28, ISSN: 0036-8075

Hu, Y.; Churchill, H. O. H.; Reilly, D. J.; Xiang, J.; Lieber, C. M. & Markus, C. M. (2007). A Ge/Si heterostructure nanowire-based double quantum dot with integrated charge sensor. *Nature Nanotechnology*, 2, 10, (October 2007) 622-625, ISSN: 1748-3387

Huang, Y.; Duan, X.; Cui, Y. & Lieber, C. M. (2002). Gallium nitride nanowire nanodevices. *Nano Letters*, 2, 2, (February 2002) 101-104, ISSN: 1530-6984

Hughes, J. L. P. & Sipe, J. E. (1996). Calculation of second-order optical response in semiconductors. *Physical Review B*, 53, 16, (April 1996) 10751-10763, ISSN: 0163-1829

Humphreys, C. J.; Galtrey, M. J.; van der Laak, N.; Oliver, R. A.; Kappers, M. J.; Barnard, J. S.; Graham, D. M. & Dawson, P. (2007). The Puzzle of Exciton Localisation in GaN-Based Structures: TEM, AFM and 3D APFIM Hold the Key. *Microscopy of semiconducting materials 2007*, *Springer Proceedings in Physics*, 120, (April 2008) 3-12, ISSN: 0930-8989

Iakoubovskii, K.; Mitsuishi, K. & Furuya, K. (2008). High-resolution electron microscopy of detonation nanodiamond. *Nanotechnology*, 19, 15, (April 2008) 155705, ISSN: 0957-4484

Ihn, S-G.; Song, J-I.; Kim, Y-H. & Lee, J. Y. (2006). GaAs nanowires on Si substrates grown by a solid source molecular beam epitaxy. *Applied Physics Letters*, 89, 5, (July 2006) 053106, ISSN: 0003-6951

Irrera, A.; Iacona, F.; Franzò, G.; Boninelli, S.; Pacifici, D.; Miritello, M.; Spinella, C.; Sanfilippo, D.; Di Stefano, G.; Fallica P. G. & Priolo, F. (2005). Correlation between

electroluminescence and structural properties of Si nanoclusters. *Optical Materials*, 27, 5, (February 2005) 1031-1040, ISSN: 0925-3467

Johansson, J.; Karlsson, L. S.; Svensson, C. P. T.; Martensson, T.; Wacaser, B. A.; Deppert, K.; Samuelson, L. & Seifert, W. (2006). Structural properties of (111)B-oriented III-V nanowires. *Nature Materials*, 5, 7, (July 2006) 574-580, ISSN: 1476-1122

Jones, R. O. & Gunnarsson, O. (1989). The density functional formalism, its applications and prospects. *Review of Modern Physics*, 61, 3, (July 1989) 689-746, ISSN: 0034-6861

Karlsson, L. S.; Dick, K. A.; Wagner, J. B.; Malm, J. O.; Deppert, K.; Samuelson, L. & Wallenberg, L. R. (2007). Understanding the 3D structure of GaAs < 111 > B nanowires. *Nanotechnology*, 18, 48, (December 2007) 485717, ISSN: 0957-4484

Kastner, M. A. (1992). The single-electron transistor. *Reviews of Modern Physics*, 64, 3, (July 1992) 849-858, ISSN: 0034-6861

Kaufman, D.; Berk, Y.; Dwir, B.; Rudra, A.; Palevski, A. & Kapon, E. (1999). Conductance quantization in V-groove quantum wires. *Physical Review B*, 59, 16, (April 1999) 10433-10436, ISSN: 1098-0121

Kim, H. S.; Hwang, S. O.; Myung, Y.; Park, J.; Bae, S. Y. & Ahn, J. P. (2008). Three-dimensional structure of helical and zigzagged nanowires using electron tomography. *Nano Letters*, 8, 2, (February 2008) 551-557, ISSN: 1530-6984

Kim, T. Y.; Lee, S. H.; Mo, Y. H.; Shim, H. W.; Nahm, K. S.; Suh, E-K.;Yang, J. W.; Lim, K. Y. & Park, G. S. (2003). Growth of GaN nanowires on Si substrate using Ni catalyst in vertical chemical vapor deposition reactor. *Journal of Crystal Growth*, 257, 1-2, (September 2003) 97-103, ISSN: 0022-0248

Klug, A. (1982). From macromolecules to biological assemblies. *Nobel lecture*, Stockholm, December 1982.

Koguchi, M.; Kakibayashi, H.; Tsuneta, R.; Yamaoka, M.; Niino, T.; Tanaka, N.; Kase, K. & Iwaki, M. (2001). Three-dimensional STEM for observing nanostructures. *Journal of Electron Microscopy*, 50, 3, (January 2001) 235-241, ISSN: 0022-0744

Kuykendall, T.; Ulrich, P.; Aloni, S. & Yang, P. (2007). Complete composition tunability of InGaN nanowires using a combinatorial approach. *Nature Materials*, 6, 12, (December 2007) 951-956, ISSN: 1476-1122

Lai, F-I.; Kuo, S. Y.; Chang, Y. H.; Huang, H. W.; Chang, C. W.; Yu, C. C.; Lin, C. F.; Kuo, H. C. & Wang, S. C. (2006). Fabrication of magnesium-doped gallium nitride nanorods and microphotoluminescence characteristics. *Journal of Vacuum Science and Technology B*, 24, 3, (May-June 2006) 1123-1126, ISSN: 1071-1023

Lazar, S.; Botton, G. A.; Wu, M-Y.; Tichelaar, F. D. & Zandbergen, H. W. (2003). Materials science applications of HREELS in near edge structure analysis and low-energy loss spectroscopy. *Ultramicroscopy*, 96, 3-4, (September 2003) 535-546, ISSN: 0304-3991

Levine, Z. H. & Allan, D. C. (1989). Linear optical-response in silicon and germanium including self-energy effects. *Physical Review Letters*, 63, 16, (October 1989) 1719-1722, ISSN: 0031-9007

Lieber, C. M. (2003). Nanoscale science and technology: Building a big future from small things. *MRS Bulletin*, 28, 7, (July 2003) 486-491, ISSN: 0883-7694

Lieber, C. M. & Wang, Z. L. (2007). Functional nanowires. *MRS Bulletin*, 32, 2, (February 2007) 99-108, ISSN: 0883-7694

Merano, M.; Sonderegger, S.; Crottini, A.; Collin, S.; Pelucchi, E.; Renucci, P.; Malko, A.; Baier, M. H.; Kapon, E.; Ganiere, J. D. & Deveaud, B. (2006). Time-resolved

cathodoluminescence of InGaAs/AlGaAs tetrahedral pyramidal quantum structures. *Applied Physics B*, 84, 1-2, (July 2006) 343-350, ISSN: 0946-2171

Midgley, P. A.; Weyland, M.; Thomas, J. M. & Johnson, B. F. G. (2001). Z-Contrast tomography: a technique in three-dimensional nanostructured analysis based on Rutherford scattering. *Chemical Communications*, 10, (February 2001), 907-908, ISSN: 1359-7345

Midgley, P. A. & Weyland, M. (2003). 3D electron microscopy in the physical science: the development of Z-contrast and EFTEM tomography. *Ultramicroscopy*, 96, 3-4, (September 2002), 413-431, ISSN: 0304-3991

Midgley, P. A.; Ward, E. P. W.; Hungría, A. B. & Thomas, J. M. (2007). Nanotomography in the chemical, biological and materials sciences. *Chemical Society Reviews*, 36, 9, (September 2007) 1477-1494, ISSN: 0306-0012

Mikkelsen, A.; Sköld, N.; Ouattara, L.; Borgström, M.; Andersen, J. N.; Samuelson, L.; Seifert, W. and Lundgren, E. (2004). Direct imaging of the atomic structure inside a nanowire by scanning tunnelling microscopy. *Nature Materials*, 3, 8, (August 2004) 519-523, ISSN: 1476-1122

Möbus, G.; Doole, R. C. & Inkson, B. J. (2003). Spectroscopic electron tomography. *Ultramicroscopy*, 96, 3-4, (September 2003) 433-451, ISSN: 0304-3991

Montoro, L. A.; Leite, M. S.; Biggemann, D.; Peternella, F. G.; Batenburg, K. J.; Medeiros-Ribeiro, G. & Ramirez, A. J. (2009). Revealing Quantitative 3D Chemical Arrangement on Ge-Si Nanostructures. *Journal of Physical Chemistry C*, 113, 21, (May 2009) 9018-9022, ISSN: 1932-7447

Morral, A. F. I.; Arbiol, J.; Prades, J. D.; Cirera, A. & Morante, J. R. (2007). Synthesis of silicon nanowires with wurtzite crystalline structure by using standard chemical vapor deposition. *Advanced Materials*, 19, 10, (May 2007) 1347-1349, ISSN: 0935-9648

Morral, A. F. I.; Colombo, C.; Abstreiter, G.; Arbiol, J. & Morante, J. R. (2008). Nucleation mechanism of gallium-assisted molecular beam epitaxy growth of gallium arsenide nanowires. *Applied Physics Letters*, 92, 6, (February 2008) 063112, ISSN: 0003-6951

Morral, A. F. I.; Spirkoska, D.; Arbiol, J.; Morante, J. R. & Abstreiter, G. (2008). Prismatic quantum heterostructures synthesized on molecular-beam epitaxy GaAs nanowires. *Small*, 4, 7, (July 2008) 899-903, ISSN: 1613-6810Nesbitt, D. J. (2007). Photonics - Charge of the light brigade. *Nature*, 450, 7173, (December 2007) 1172-1773, ISSN: 0028-0836

Pal, S.; Ingale, A.; Dixit, V. K.; Sharma, T. K.; Porwal, S.; Tiwari, P. & Nath, A. K. (2007). A comparative study on nanotextured high density Mg-doped and undoped GaN. *Journal of Applied Physics*, 101, 4, (February 2007) 044311, ISSN: 0021-8979

Pan, Y. H.; Sader, K.; Powell, J. J.; Bleloch, A.; Gass, M.; Trinick, J.; Warley, A. , Li, A.; Brydson, R. & Brown, A. (2009). 3D morphology of the human hepatic ferritin mineral core: New evidence for a subunit structure revealed by single particle analysis of HAADF-STEM images. *Journal of Structural Biology*, 166, 1, (April 2009) 22-31, ISSN: 1047-8477

Park, Y. S.; Na, J. H.; Taylor, R. A.; Park, C. M.; Lee, K. H. & Kang, T. W. (2006). The recombination mechanism of Mg-doped GaN nanorods grown by plasma-assisted molecular-beam epitaxy. *Nanotechnology*, 17, 3, (February 2006) 913-916, ISSN: 0957-4484

Park, Y. S.; Park, C. M.; Park, C. J.; Cho, H. Y.; Lee, S. J.; Kang, T. W.; Lee, S. H.; Oh, J-E.; Yoo, K-H. & Son, M.-S. (2006). Electron trap level in a GaN nanorod p-n junction grown by molecular-beam epitaxy. *Applied Physics Letters*, 88, 19, (May 2006) 192104, ISSN: 0003-6951

Penczek, P.; Marko, M.; Buttle, K. & Frank, J. (1995). Double-tilt electron tomography. *Ultramicroscopy*, 60, 3, (October 1995), 393-410, ISSN: 0304-3991

Perdew, J. P.; Burke, K. & Ernzerhof, M. (1996). Generalized gradient approximation made simple. *Physical Review Letters*, 77, 18, (October 1996) 3865-3868, ISSN: 0031-3844

Pettersson, H.; Tragardh, J.; Persson, A. I.; Landin, L.; Hessman, D. & Samuelson, L. (2006). Infrared photodetectors in heterostructure nanowires. *Nano Letters*, 6, 2, (February 2006) 229-232, ISSN: 1530-6984

Qian, F.; Li, Y.; Gradeak, S.; Park, H.-G.; Dong, Y.; Ding, Y.; Wang, Z. L. & Lieber, C. M. (2008). Multi-quantum-well nanowire heterostructures for wavelength-controlled lasers. *Nature Materials*, 7, 9, (September 2008) 701-706, ISSN: 1476-1122

Qin, Y.; Wang, X. D. & Wang, Z. L. (2008). Microfibre-nanowire hybrid structure for energy scavenging. *Nature*, 451, 7180, (February 2008) 809-U5, ISSN: 0028-0836

Radon, J. (1917). Über die Bestimmung von Funktionen durch ihre Integralwerte längs gewisser Mannigfaltigkeiten. *Berichte Sachsische Akademie der Wissenschaften Leipzig*, 69, (1917) 262-277, ISSN: 1867-7061

Read, A. J. & Needs, R. J. (1991). Calculation of optical matrix-elements with nonlocal pseudopotentials. *Physical Review B*, 44, 23, (December 1991), 13071-13073, ISSN: 0163-3844

Samuelson, L.; Thelander, C.; Bjork, M. T.; Borgstrom, M.; Deppert, K.; Dick, K. A.; Hansen, A. E.; Martensson, T.; Panev, N.; Persson, A. I.; Seifert, W.; Skold, N.; Larsson, M. W. & Wallenberg, L. R. (2004). Semiconductor nanowires for 0D and 1D physics and applications. *Physica E*, 25, 2-3, (November 2004) 313-318, ISSN: 1386-9477

Sanchez, A. M.; Beanland, R.; Papworth, A. J.; Goodhew, P. J. & Gass, M. H. (2006). Nanometer-scale strain measurements in semiconductors. *Applied Physics Letters*, 88, 5, (January 2006) 051917, ISSN: 0003-6951

Schedelbeck, G.; Wegscheider, W.; Bichler, M. & Abstreiter, G. (1997). Coupled quantum dots fabricated by cleaved edge overgrowth: From artificial atoms to molecules. *Science*, 278, 5344, (December 1997) 1792-1795, ISSN: 0036-8075

Shen, Y. G.; Mai, Y. W.; McKenzie, D. R. , Zhang, Q. C.; McFall, W. D. & McBride, W. E. (2000). Composition, residual stress, and structural properties of thin tungsten nitride films deposited by reactive magnetron sputtering. *Journal of Applied Physics*, 88, 3, (August 2000) 1380-1388, ISSN: 0021-8979

Shorubalko, I.; Leturcq, R.; Pfund, A.; Tyndall, D.; Krischek, R.; Schön, S. & Ensslin, K. (2008). *Nanoletters*, 8, 2, (February 2008) 382-385, ISSN: 1530-6984

Sigle, W. (2005). Analytical transmission electron microscopy. *Annual Review of Materials Research*, 35, (December 2005) 239-314, ISSN: 1531-7331

Soler, J. M.; Artacho, E.; Gale, J. D.; Garcia, A.; Junquera, J.; Ordejon. P. & Sanchez-Portal, D. (2002). The SIESTA method for ab initio order-N materials simulation. *Journal of Physics: Condensed Matter*, 14, 11, (March 2002) 2745-2778, ISSN: 0953-8984

Stern, E.; Klemic, J. F.; Routenberg, D. A.; Wyrembak, P. N.; Turner-Evans, D. B.; Hamilton, A. D.; LaVan, D. A.; Fahmy, T. M. & Reed, M. A. (2007). Label-free

immunodetection with CMOS-compatible semiconducting nanowires. *Nature*, 445, 7127, (February 2007) 519-522, ISSN: 0028-0836

Thelander, C.; Agarwal, P.; Brongersma, S.; Eymery, J.; Feiner, L. F.; Forchel, A.; Scheffler, M.; Riess, W.; Ohlsson, B. J.; Gosele, U. & Samuelson, L. (2006). Nanowire-based one-dimensional electronics. *Materials Today*, 9, 10, (October 2006) 28-35, ISSN: 1369-7021

Thunich, S.; Prechtel, L.; Spirkoska, D.; Abstreiter, G.; Morral, A. F. I. & Holleitner, A. W. (2009). Photocurrent and photoconductance properties of a GaAs nanowire. *Applied Physics Letters*, 95, 8, (August 2009) 083111, ISSN: 0003-6951

Topuria, T.; Browning, N. D. & Ma, Z. (2003). Characterization of ultrathin dopant segregation layers in nanoscale metal-oxide-semiconductor field effect transistors using scanning transmission electron microscopy. *Applied Physics Letters*, 83, 21, (November 2003) 4432-4434, ISSN: 0003-6951

van den Broek, W.; Verbeeck, J.; De Backer, S.; Scheunders, P. & Schryvers, D. (2006). Acquisition of the EELS data cube by tomographic reconstruction. *Ultramicroscopy*, 106, 4-5, (March 2006) 269-276, ISSN: 0304-3991

Verheijen, M. A.; Algra, R. E.; Borgstrom, M. T.; Immink, G.; Sourty, E.; van Enckevort, W. J. P.; Vlieg, E. & Bakkers, E. P. A. M. (2007). Three-dimensional morphology of GaP-GaAs nanowires revealed by transmission electron microscopy tomography. *Nano Letters*, 7, 10, (October 2007) 3051-3055, ISSN: 1530-6984

Wang, X. D.; Song, J.; Liu, J. & Wang, Z. L. (2007). Direct-current nanogenerator driven by ultrasonic waves. *Science*, 316, 5821, (April 2006) 102-105, ISSN: 0036-8075

Wagner, R. S. & Ellis, W. C. (1964). Vapor-liquid-solid mechanism of single crystal growth (new method growth catalysis from impurity whisker epitaxial + large crystals Si e). *Applied Physics Letters*, 4, 5, (March 1964) 89-90, ISSN: 0003-6951

Wang, J. F.; Gudiksen, M. S.; Duan, X. F.; Cui, Y. & Lieber, C. M. (2001). Highly polarized photoluminescence and photodetection from single indium phosphide nanowires. *Science*, 293, 5534, (August 2001) 1455-1457, ISSN: 0036-8075

Wang, W. U.; Chen, C.; Lin, K. H.; Fang, Y. & Lieber, C. M. (2005). Label-free detection of small-molecule-protein interactions by using nanowire nanosensors. *Proceedings Of The National Academy of Sciences of The United States of America*, 102, 9, (March 2005) 3208-3212, ISSN: 0027-8424

Wegscheider, W.; Pfeiffer, L. N.; Dignam, M. M.; Pinczuk, A.; West, K. W.; McCall, S. L. & Hull, R. (1993). Lasing from excitons in quantum wires. *Physical Review Letters*, 71, 24, (December 1993) 4071-4074, ISSN: 0031-9007

Wegscheider, W.; Pfeiffer, L.; Dignam, M.; Pinzcuk, A.; West, K. & Hull, R. (1994). Lasing in lower-dimensional structures formed by cleaved edge overgrowth. *Semiconductor Science and Technolology*, 9, 11, (November 1994) 1933-1938, ISSN: 0268-1242

Wegscheider, W.; Rother, M.; Schedelbeck, G.; Bichler, M. & Abstreiter, G. (1999). Optical and transport properties of low-dimensional structures fabricated by cleaved edge overgrowth. *Microelectronic Engineering*, 47, 1-4, (June 1999) 215-219, ISSN: 0167-9317

Weyland, M. (2002). Electron tomography of catalysts. *Topics in Catalysis*, 21, 4, (December 2002) 175-183, ISSN: 1022-5528

Xin, Y.; James, E. M.; Arslan, I.; Sivananthan, S.; Browninga, N. D.; Pennycook, S. J.; Omnes, F.; Beaumont, B.; Faurie, J. & Gibart, P. (2000). Direct experimental observation of

the local electronic structure at threading dislocations in metalorganic vapor phase epitaxy grown wurtzite GaN thin films. *Applied Physics Letters*, 76, 4, (January 2000) 466-468, ISSN: 0003-6951

Yang, P. D. (2005). The chemistry and physics of semiconductor nanowires. *MRS Bulletin*, 30, 2, (February 2005) 85-91, ISSN: 0883-7694

Zhong, Z. H.; Qian, F.; Wang & D. Lieber, C. M. (2003). Synthesis of p-type gallium nitride nanowires for electronic and photonic nanodevices. *Nanoletters*, 3, 3, (March 2003) 343-346, ISSN: 1530-6984

Nanowires

Edited by Paola Prete

ISBN 978-953-7619-79-4
Hard cover, 414 pages
Publisher InTech
Published online 01, February, 2010
Published in print edition February, 2010

This volume is intended to orient the reader in the fast developing field of semiconductor nanowires, by providing a series of self-contained monographs focusing on various nanowire-related topics. Each monograph serves as a short review of previous results in the literature and description of methods used in the field, as well as a summary of the authors recent achievements on the subject. Each report provides a brief sketch of the historical background behind, the physical and/or chemical principles underlying a specific nanowire fabrication/characterization technique, or the experimental/theoretical methods used to study a given nanowire property or device. Despite the diverse topics covered, the volume does appear as a unit. The writing is generally clear and precise, and the numerous illustrations provide an easier understanding of the phenomena described. The volume contains 20 Chapters covering altogether many (although not all) semiconductors of technological interest, starting with the IV-IV group compounds (SiC and SiGe), carrying on with the binary and ternary compounds of the III-V (GaAs, AlGaAs, GaSb, InAs, GaP, InP, and GaN) and II-VI (HgTe, HgCdTe) families, the metal oxides (CuO, ZnO, ZnCoO, tungsten oxide, and PbTiO3), and finishing with Bi (a semimetal).

InTech Europe
University Campus STeP Ri
Slavka Krautzeka 83/A
51000 Rijeka, Croatia
Phone: +385 (51) 770 447
Fax: +385 (51) 686 166
www.intechopen.com

InTech China
Unit 405, Office Block, Hotel Equatorial Shanghai
No.65, Yan An Road (West), Shanghai, 200040, China
中国上海市延安西路65号上海国际贵都大饭店办公楼405单元
Phone: +86-21-62489820
Fax: +86-21-62489821

IntechOpen